Murine M1 macrophages are among the direct responders to tumor-derived extracellular cGAMP and their human counterparts use SLC46A2 to import cGAMP

Anthony F. Cordova[1,2,4], Christopher Ritchie[1,2,4], Volker Böhnert[1,2], Rachel E. Mardjuki[2,3], Lingyin Li[1,2,5]

[1]Department of Biochemistry, [2]Institute of Chemistry, Engineering, and Medicine for Human Health (ChEM-H), [3]Department of Chemistry, Stanford University, Stanford, CA 94305, USA, [4]These authors contributed equally, [5]Corresponding Author and Lead Contact: lingyinl@stanford.edu

Summary

Administration of exogenous CDNs to activate the cGAMP-STING pathway is a promising therapeutic strategy to unleash the full potential of cancer immunotherapy. This strategy mirrors the role of endogenous extracellular cGAMP, which we recently described as an immunotransmitter exported by cancer cells and imported into local responder cells of unknown identities to promote anti-tumoral immunity, with irradiation enhancing this effect. Here, in low-dose irradiated murine tumors, we identified $CD4^+$ T cells, M1 macrophages, and $NKG2D^{Low}$ NK cells as cGAMP responder cells that have decreased STING activation upon depletion of extracellular cGAMP. At higher doses of radiation, extracellular cGAMP promoted the death of T cells and macrophages. Furthermore, we identified the orphan protein SLC46A2 as the dominant importer of cGAMP and select bacterial CDNs in human macrophages and monocytes. Together, we provide the first cellular and molecular mechanisms of cGAMP as an immunotransmitter, paving the way for effective STING pathway therapeutics.

Introduction

Cancer immunotherapy has revolutionized the way in which cancer is treated, enabling physicians to now cure previously terminal diseases (Sharma and Allison, 2015). Although the majority of approved therapies target the adaptive immune system (particularly T cells), activation of innate immune pathways is a prerequisite for these therapies to be effective. As such, there is growing interest in developing therapies that also target the innate immune system. In particular, the cGAMP-STING innate immune pathway is a promising anticancer target; cGAMP analogs show remarkable efficacy in murine models of cancer (Corrales et al., 2015; Curran et al., 2016) and these analogs are currently in clinical trials for solid tumors (NCT02675439, NCT03172936, and NCT03937141).

The cGAMP-STING pathway is activated by the presence of double-stranded DNA (dsDNA) in the cytosol (Sun et al., 2013), which can result from viral infection, cell damage, or chromosomal instability inherent to cancer. Upon detection of cytosolic dsDNA, the enzyme cyclic-GMP-AMP synthase (cGAS) synthesizes the cyclic dinucleotide (CDN) second messenger 2'3'-cyclic-GMP-AMP (cGAMP) (Ablasser et al., 2013a; Gao et al., 2013; Wu et al., 2013). cGAMP binds and activates the ER membrane protein Stimulator of Interferon Genes (STING). STING then activates TBK1, a kinase, and IRF3, a transcription factor, resulting in the expression of inflammatory cytokines (Ishikawa et al., 2009). Of particular interest, the type I interferon (IFN-I) class of cytokines is necessary for cGAMP-mediated activation of T cells and effective anti-tumoral immunity (Deng et al., 2014).

While cGAMP leads to a strong IFN-I response in some cell types, there is mounting evidence that the effects of cGAMP signaling are cell-type specific. For example, it has been shown that T cells die in response to cGAMP signaling (Cerboni et al., 2017; Gulen et al., 2017; Larkin et al., 2017). Additionally, a recent study showed that cGAMP signaling in different cell types in the mouse lung led to different levels of IFN-I production, with some cell types unable to produce enough IFN-I for effective immunity (Wang et al., 2020). The differential response to

cGAMP across cell types suggests that, in some conditions, cGAMP transfer to strong IFN-I producing cells could result in a more effective immune response. In line with this, we and others have demonstrated in murine cancer models that cGAMP acts as an immunotransmitter that is transferred from cancer cells to host cells (Carozza et al., 2020; Zhou et al., 2020b). Since genomic instability and cytosolic dsDNA are hallmarks of cancer (Harding et al., 2017; Mackenzie et al., 2017), cancer cells often constitutively synthesize cGAMP. However, for many cancer cells STING signaling does not result in effective production of IFN-Is (Bakhoum and Cantley, 2018; Bakhoum et al., 2018; Xia et al., 2016). Thus, in order for an effective immune response to occur, cGAMP must be secreted from cancer cells into the extracellular space (Carozza et al., 2020), where it can then be imported into the cytosol of responder cells.

While it is known that this transfer of cGAMP ultimately results in downstream immune activation, it is unknown which cell types directly respond to tumor-derived extracellular cGAMP. Several studies have suggested that $CD11c^+$ dendritic cells are the cGAMP-sensing cells in tumors (Andzinski et al., 2016; Carozza et al., 2020; Laursen et al., 2018), while others have identified macrophages (Zhou et al., 2020b), NK cells (Marcus et al., 2018; Nicolai et al., 2020), endothelial cells (Demaria et al., 2015), and $CD11b^+$ myeloid cells (Marcus et al., 2018). However, these studies either relied on exogenous cGAMP administration or did not directly measure activation of the STING pathway in different cell types. As a result, the identity of cGAMP responder cells *in vivo* remains an open question. Furthermore, the cGAMP import mechanism of these responder cells is also unknown. It is clear that import mechanisms differ by cell type and context, and although multiple cGAMP transporters have been identified (Lahey et al., 2020; Luteijn et al., 2019; Ritchie et al., 2019; Zhou et al., 2020a), it is unknown which ones are used by cGAMP responder cells. Identifying the responder cells to endogenous extracellular cGAMP and characterizing their cGAMP transport mechanisms will be crucial to understanding the role of the STING pathway in the antitumoral immune response and to rationally design more effective CDN-based therapeutics.

Here, we depleted extracellular cGAMP from a murine tumor model in order to identify direct cGAMP responders in the tumor microenvironment. We found that subsets of T cells, macrophages, and NK cells directly respond to tumor-derived extracellular cGAMP by activating the STING pathway and producing IFN-Is. Additionally, we identified SLC46A2, an orphan solute carrier transporter protein, as the primary cGAMP importer in human M1 macrophages and their monocyte precursors.

Results

Tumor-derived extracellular cGAMP alters the immune composition of 4T1 murine mammary tumors

We previously demonstrated that cancer cells are able to synthesize and export cGAMP *in vitro* (Carozza et al., 2020); however, extracellular cGAMP has not been directly detected within tumors. In order to demonstrate that tumors are able to synthesize and export cGAMP *in vivo*, we established orthotopic 4T1-luciferase mammary tumors in BALB/c mice. To determine if ionizing radiation promotes cGAMP synthesis in tumors, as has been previously suggested (Carozza et al., 2020; Deng et al., 2014), established tumors were then irradiated with 0, 12, or 20 Gy. After 24 hours, the tumors were extracted from the mice and incubated in cell culture media to collect cGAMP exported by the tumors. The ENPP1 inhibitor STF-1084 (Carozza et al., 2020) was used to prevent degradation of extracellular cGAMP once it had been exported. After 24 hours the conditioned media was collected and extracellular cGAMP was quantified (Mardjuki et al., 2020). All tumors exported cGAMP in the range of 20-90 pmol per gram of tumor, suggesting that ionizing radiation is not required for cGAMP production and export (**Figure 1A**).

Having demonstrated that tumors can synthesize and export cGAMP, we next sought to identify the changes in the immune composition of the tumor that were mediated by tumor-

derived extracellular cGAMP. Orthotopic 4T1-luciferase tumors were established in BALB/c mice, and again the tumors were irradiated with 0, 12, or 20 Gy. In order to specifically isolate the effects of extracellular cGAMP, we depleted extracellular cGAMP 24 hours after irradiation with intratumoral injections of soluble STING protein, and after an additional 24 hours tumors were extracted and analyzed by flow cytometry (**Figure 1B, S1**). A mutant version of STING that does not bind cGAMP (R237A) (Carozza et al., 2020) was used as a non-binding control. For clarity, we will hereafter refer to tumors injected with non-binding STING as having extracellular cGAMP and those injected with neutralizing STING as not having extracellular cGAMP.

Radiation by itself led to a decrease in total cell viability (**Figure S2A**) as well as an increase in immune cell infiltration (**Figure 1C**). In contrast, the presence of extracellular cGAMP had no effect on either total cell viability or immune cell infiltration. However, at the highest dose of radiation (20 Gy), the presence of extracellular cGAMP decreased specific immune cell populations within the tumor microenvironment. Specifically, extracellular cGAMP decreased the percentage of T cells in tumors irradiated with 20 Gy (**Figure 1D-E**) and this decrease was present in both $CD4^+$ and $CD8^+$ T cells (**Figure S2B-C**). However, the ratio of $CD4^+$ to $CD8^+$ T cells was unchanged by extracellular cGAMP (**Figure S2D**). This decrease in T cells was likely due to T cell death in response to extracellular cGAMP, as there was a lower percentage of living T cells in the tumors exposed to extracellular cGAMP at 20 Gy (**Figure 1F**). In addition to T cells, extracellular cGAMP also resulted in a decrease in the percentage of $F4/80^+$ macrophages in tumors receiving 20 Gy (**Figure 1G**). However, extracellular cGAMP had no significant effect on the population size of the other immune cells we examined, including $CD11c^+$ dendritic cells (**Figure S2E**), $CD19^+$ B cells (**Figure S2F**), $CD335^+$ NK cells (**Figure S2G**) and Ly-$6C^+$ monocyte-lineage cells and endothelial cells (Jutila et al., 1988) (**Figure S2H**). Taken together, these data suggest that tumor-derived extracellular cGAMP elicits a specific immune response within the tumor rather than a global change in all immune cells (**Figure 1H**).

Intratumoral $CD4^+$ T cells are direct responders to tumor-derived extracellular cGAMP

Having established that tumor-derived extracellular cGAMP induces immune changes within the tumor microenvironment, we next sought to determine whether these changes were due to a direct response to extracellular cGAMP, or whether they were a downstream secondary response. To this end, we probed the tumor samples for phosphorylated STING (pSTING) and phosphorylated IRF3 (pIRF3), which are both markers of STING pathway activation (Ablasser et al., 2013b; Konno et al., 2013). Any changes in pSTING and pIRF3 signal between samples treated with neutralizing or non-binding STING must have been due to a direct response to extracellular cGAMP. Additionally, we probed for the IFN-Is, interferon alpha (IFNα) and interferon beta (IFNβ), which are not specific for STING pathway activation, but are the functional consequences of its activation. Because radiation increases immune cell infiltration of the tumor, all subsequent analyses were performed on tumors receiving 12 Gy of radiation.20 Gy was avoided due to the potentially toxic effects on T cells and macrophages.

Flow cytometry analysis revealed that T cells directly respond to endogenous extracellular cGAMP within tumors. T cells had increased pSTING (**Figure 2A-B**) and pIRF3 (**Figure 2C-D**) signal in the presence of extracellular cGAMP, indicating higher levels of STING pathway activation within these cells. Furthermore, T cells also had higher expression of both IFNα and IFNβ in the presence of extracellular cGAMP (**Figure S3**). These effects were primarily driven by $CD4^+$ T cells (**Figure 2E**), as $CD8^+$ T cells did not show any significant changes in pSTING, pIRF3, or IFNα; however, the changes in IFNβ were due to $CD8^+$ T cells (**Figure 2F**). Taken together, this data suggests that intratumoral $CD4^+$ T cells are direct cGAMP responders, while $CD8^+$ T cells likely play a downstream role in cGAMP-mediated immune activation.

Intratumoral macrophages and NK cells directly respond to tumor-derived extracellular cGAMP

Having identified T cells as direct cGAMP responders, we next turned our analysis to other immune cell types within the tumor. Numerous studies have identified macrophages as a key cell type in the STING-mediated antitumoral immune response (Cheng et al., 2018; Ohkuri et al., 2017; Zhou et al., 2020b). Here, we provide evidence that F4/80^{+} macrophages directly respond to tumor-derived extracellular cGAMP. Macrophages had increased pSTING (**Figure 3A-B**) and pIRF3 (**Figure S4A**) signal in the presence of extracellular cGAMP, as well as increased IFNα and IFNβ (**Figure S4B**).

Macrophages comprise a wide range of cell states with varied and sometimes opposing roles, ranging from anti-tumoral M1 macrophages (Sinha et al., 2005) to pro-tumoral M2 macrophages (also known as tumor-associated macrophages (TAMs)) (Kurahara et al., 2011; Steidl et al., 2010). To distinguish between these macrophage states, we used the established maker CD206 (also known as MMR or MRC1), which is highly expressed in M2 macrophages (CD206^{High}) and lowly expressed in M1 macrophages (CD206^{Low}) (Murray et al., 2014; Porcheray et al., 2005). We found that CD206^{Low} macrophages directly responded to tumor-derived extracellular cGAMP (**Figure 3C-E**), while CD206^{High} macrophages did not (**Figure S4C-E**). In addition, the number of CD206^{Low} macrophages decreased as a percentage of total macrophages (**Figure 3F)**, possibly due to STING activation-induced death (Gaidt et al., 2017). It is also possible that the CD206^{Low} population converted into CD206^{High} macrophages, as we observed a statistically insignificant increase in the absolute number of CD206^{High} macrophages in the tumor microenvironment (**Figure S4F-G**); however, there has been evidence that cGAMP mediates the opposite conversion of M2 to M1 macrophages (Downey et al., 2014). Ly-6C^{+} cells, which are the monocytic precursors to macrophages (Jutila et al., 1988), also had increased STING pathway activation in response to extracellular cGAMP, but did not show an increase in IFNα and IFNβ production (**Figure 3G, S4H-I**). Because STING activation typically precedes IFNα and IFNβ production by hours, it is possible that Ly-6C^{+} cells arrived later or took up cGAMP with slower kinetics. Alternatively, it is possible that STING activation in Ly-6C^{+} cells resulted in their differentiation prior to IFN-I production.

In addition to macrophages, NK cells have also been implicated in the cGAMP-mediated antitumoral immune response (Marcus et al., 2018; Nicolai et al., 2020). We found that NK cells (marked by CD335^{+}) also had higher STING pathway activation (**Figure 4A-B**, **S5A**) and IFN-I production (**Figure 4C**) in the presence of tumor-derived extracellular cGAMP within the tumor. NKG2D (also known as CD314) is an activating receptor that has increased expression on mature NK cells (Gilfillan et al., 2002; Huntington et al., 2007). NKG2D^{Low} NK cells showed an increase in STING pathway activation (**Figure 4D-E**) and IFNα and IFNβ production (**Figure S5C**) in the presence of extracellular cGAMP, suggesting that the NKG2D^{Low} NK cells are the direct cGAMP responders. NKG2D^{High} NK cells had an increase in IFNα and IFNβ production (**Figure S5D**) without an increase in STING pathway activation (**Figure S5B**), suggesting that they are indirectly activated by extracellular cGAMP. As with the macrophages, the responder cell population (NKG2D^{Low}) decreased relative to the non-responder population when exposed to extracellular cGAMP (**Figure 4F**), possibly due to death or differentiation into NKG2D^{high} cells (**Figure S5E**).

Although there has been considerable evidence that dendritic cells play a vital role in the anti-tumoral immune response (Andzinski et al., 2016; Carozza et al., 2020; Laursen et al., 2018), there were no differences in STING pathway activation in the presence or absence of tumor-derived extracellular cGAMP (**Figure S5F**), suggesting that their role in anti-tumoral immunity is downstream of a direct cGAMP responder cell. Likewise, there were no differences observed in B cells (**Figure S5G**). Together, these results demonstrate that only a specific subsets of immune cells within the tumor directly respond to tumor-derived extracellular

cGAMP, with downstream effector cells being important for the subsequent immune response (**Figure 4G**).

CD14$^+$ monocytes express high levels of the uncharacterized transporter SLC46A2

Having identified the cell types that directly respond to tumor-derived extracellular cGAMP, we next sought to identify the mechanism by which these cells internalize and respond to cGAMP. As there is evidence that cGAMP import mechanisms are not conserved between mice and humans (Luteijn et al., 2019; Ritchie et al., 2019), we continued our investigation in human primary cells and cell lines, rather than in mice, as this line of inquiry has greater therapeutic potential. Given the well-established anti-tumoral properties of M1 macrophages, we decided to focus our investigation on these cells and their precursors, CD14$^+$ monocytes, which are easily obtainable from whole blood.

We previously characterized the reduced folic acid carrier SLC19A1 as an importer of cGAMP (Ritchie et al., 2019). However, we determined that SLC19A1 only plays a limited role as a cGAMP importer in CD14$^+$ monocytes, as the SLC19A1 inhibitor methotrexate (MTX) had little effect on their extracellular cGAMP signaling (Ritchie et al., 2019). Despite this, another inhibitor of SLC19A1, sulfasalazine (SSZ), strongly inhibited extracellular cGAMP signaling in CD14$^+$ monocytes (**Figure 5A**). This suggests that SSZ is inhibiting an unknown cGAMP transporter in CD14$^+$ monocytes. Furthermore, given that we previously reported that SSZ does not inhibit cGAMP signaling in the monocyte-derived U937 *SLC19A1*$^{-/-}$ cells (Ritchie et al., 2019), it appears that U937 cells do not express this unknown cGAMP transporter (**Figure 5B**). Thus, to identify potential cGAMP transporters, we compared expression levels of transmembrane transporters between CD14$^+$ monocytes and U937 cells using published microarray data (Gebhard et al., 2010) (**Figure 5C**). Of particular interest was *SLC46A2*, which encodes an uncharacterized transmembrane transporter that is highly expressed in CD14$^+$ monocytes but not in U937 cells. Given that SLC46A2 is closely related to the proton-coupled folic acid transporter SLC46A1, a known target of SSZ, we reasoned that SLC46A2 may be the cGAMP transporter in CD14$^+$ monocytes.

Both human and mouse SLC46A2 are cGAMP transporters

In order to evaluate the potential role of human SLC46A2 protein as a cGAMP importer, we created a lentiviral vector encoding a C-terminally FLAG-tagged SLC46A2 under the control of a doxycycline inducible promoter (tet-SLC46A2-FLAG). This vector was transduced into U937 cells that had *SLC19A1* knocked out to reduce background cGAMP uptake levels (U937-tet-SLC46A2-FLAG). Using this cell line, we found that induction of SLC46A2-FLAG greatly increased the response to extracellular cGAMP (**Figure 5D**). While these data suggest that SLC46A2 is a cGAMP importer, it is possible that SLC46A2 is potentiating extracellular cGAMP signaling downstream of cGAMP import. To rule out this possibility, we evaluated the effect of SLC46A2 induction on the response to intracellular cGAMP that had been electroporated into cells (**Figure 5E**). In contrast to extracellular cGAMP signaling, SLC46A2 had no effect on intracellular cGAMP signaling, suggesting that SLC46A2 is a direct cGAMP importer (**Figure 5F**).

Although SLC19A1 is a cGAMP transporter in several human cell lines, the murine homolog of SLC19A1 (mSlc19a1) has not been identified as a cGAMP transporter in any mouse cell lines or primary cells (Luteijn et al., 2019; Ritchie et al., 2019). Consistent with this, overexpression of mSlc19a1 did not affect the response to extracellular cGAMP, indicating that mSlc19a1 is unlikely to be a cGAMP transporter (**Figure S6A**). In contrast, overexpression of the murine homolog mSlc46a2 strongly increased the response to extracellular cGAMP **(Figure 5G**) but did not increase the response to electroporated, intracellular cGAMP (**Figure 5H**). These data show that unlike SLC19A1, the ability of SLC46A2 to import cGAMP is conserved between mice and humans.

SLC46A2 selectively imports other CDNs

Given the chemical similarity across different CDNs, we tested whether SLC46A2 could import other CDNs in addition to cGAMP. Multiple synthetic CDNs, including 2'3'-bisphosphothioate-cGAMP (2'3'-cG^{S}A^{S}MP) and the investigative new drug 2'3'-bisphosphothioate-cyclic-di-AMP (2'3'-CDA^{S}), have hydrolysis-resistant phosphothioate bonds in place of phophodiester backbones. We found that induction of SLC46A2 increased the response to both 2'3'-cG^{S}A^{S}MP and 2'3'-CDA^{S}, indicating that SLC46A2 can import substrates with a phosphothioate backbone (**Figure 6A-B**). While mammalian cGAMP contains both a 2'-5' and a 3'-5' phosphodiester bond, bacterial CDNs contain two 3'-5' phosphodiester bonds. Induction of SLC46A2 increased response to two bacterial CDNs, 3'3'-cGAMP and 3'3'-CDA (**Figure 6C-D**). Interestingly, SLC46A2 induction did not increase the response to another bacterial CDN, 3'3'-CDG (**Figure 6E**), demonstrating that SLC46A2 requires adenine rings to recognize CDNs but can tolerate diverse backbone linkages.

SLC46A2 is the dominant cGAMP importer in CD14^{+} monocytes and monocyte-derived M1 macrophages

To test whether SLC46A2 is the dominant cGAMP importer in primary human monocytes, we took advantage of the small molecule inhibitor SSZ, which inhibited the effect of SLC46A2 induction on extracellular cGAMP signaling (**Figure 7A**). Comparing inhibition of extracellular cGAMP signaling across a range of SSZ concentrations in CD14^{+} monocytes and dox-induced U937-tet-SLC46A2-FLAG cells yielded inhibition curves with similar IC_{50} values, strongly suggesting that SLC46A2 is the target of SSZ in CD14^{+} monocytes (**Figure 7B**). In support of this, a ~50% knockdown of *SLC46A2* with CRISPR/Cas9 in CD14^{+} monocytes resulted in a corresponding ~50% reduction in pIRF3 in response to extracellular cGAMP (**Figure 7C**). Taken together, these data indicate that SLC46A2 is the dominant cGAMP importer in CD14^{+} monocytes.

Given that SLC19A1 and SLC46A2 are both inhibited by SSZ, we next tested whether other known inhibitors of SLC19A1 also inhibit SLC46A2. However, none of the competitive inhibitors of SLC19A1 (MTX, reduced folic acid, and oxidized folic acid) significantly inhibited SLC46A2-mediated cGAMP signaling (**Figure S7A-C**). The SSZ metabolites 5-aminosalicylic acid (5-ASA) and sulfapyridine (SP) are thought to be the therapeutically active molecules when SSZ is used to treat the inflammatory disorders inflammatory bowel disease and rheumatoid arthritis, respectively (Smedegard and Bjork, 1995). Since the mechanisms of action of these metabolites are unknown, we tested whether 5-ASA or SP inhibited extracellular cGAMP signaling through SLC46A2. We found that 5-ASA did not reduce cGAMP signaling through SLC46A2 and SP only weakly reduced cGAMP signaling (**Figure S7D**), suggesting that these metabolites do not act by inhibiting SLC46A2.

Unlike its human counterpart, mSlc46a2 was not strongly inhibited by SSZ or SLC19A1 inhibitors (**Figure S7E**). In addition, while the ability of SLC46A2 homologs to transport cGAMP appears to be conserved between species, expression levels of SLC46A2 in different cell types vary. In human immune cells, the *SLC46A2* transcript is highly expressed in monocytes and pre-DCs (**Figure S7F**). However, in murine immune cells, *Slc46a2* is poorly expressed (Gebhard et al., 2010) (**Figure S7G**). In addition, we found that murine macrophages isolated from tumors do not express appreciable levels of *Slc46a2* transcript (**Figure S7H**). These data suggest that cell-type expression of cGAMP transporters varies across species and that *Slc46a2* is likely not the dominant cGAMP transporter in the mouse tumor microenvironment.

Given that CD14^{+} monocytes use SLC46A2 as their dominant cGAMP importer, we next sought to determine whether M1 macrophages and other monocyte-derived cells use SLC46A2 as well. Freshly isolated CD14^{+} monocytes were differentiated into either M1 macrophages, M2 macrophages, or dendritic cells using an established *in vitro* protocol (Zarif et al., 2016) and the

effects of MTX and SSZ on extracellular cGAMP signaling were evaluated. For all three cell types, MTX did not inhibit extracellular cGAMP signaling, indicating that SLC19A1 is not used as a cGAMP importer by these cell types. In contrast, SSZ inhibited extracellular cGAMP signaling in all three cell types, with M1 macrophages being the most sensitive to SSZ and M2 macrophages being the least sensitive (**Figure 7D**). These data suggest that monocyte-derived primary cells also use SLC46A2 as a cGAMP importer, with greatest utilization in M1 macrophages.

Discussion

In this study we demonstrated that tumors synthesize and export cGAMP *ex vivo* and that multiple cell types import extracellular cGAMP in the tumor microenvironment, with M1 macrophages and NK cells as the primary cGAMP responders. In addition, we identified the previously uncharacterized transporter SLC46A2 as the dominant cGAMP importer in human M1 macrophages and monocyte precursor cells.

This study highlights cell-type specific responses to extracellular cGAMP signaling. While extracellular cGAMP signaling in M1 macrophages and NK cells resulted in increased IFN-I production, extracellular cGAMP signaling was toxic to T cells when combined with ionizing radiation. There is a substantial body of evidence linking STING activation to immune cell death or antiproliferation (Cerboni et al., 2017; Gaidt et al., 2017; Gulen et al., 2017; Larkin et al., 2017; Tang et al., 2016); indeed, 2'3'-CDA^{S}, one of the cGAMP analogs in clinical trials, has a narrow therapeutic window due to T cell ablation at higher doses (Sivick et al., 2018). Consequently, the impact of STING signaling on T cell viability should be considered when combining radiation, STING agonists, and/or CTLA-4/PD-1 checkpoint inhibitor therapies, which are dependent on T cells for their efficacy (Blank et al., 2004; Iwai et al., 2002; Leach et al., 1996; Shrikant et al., 1999).

While M1 macrophages and NKG2D^{Low} NK cells act as responder cells to extracellular cGAMP, their counterparts (M2 macrophages and NKG2D^{High} NK cells) do not respond to endogenous levels of tumor-derived extracellular cGAMP. Furthermore, extracellular cGAMP increased the amount of non-responder cells in tumors relative to their responder cell counterpart. It is possible that this is due to STING-activation induced death of the responder cells, or perhaps the responder cells are converting to non-responder cell populations; further studies will be required to differentiate between these two models. Instead, we focused our efforts on explaining why there are cell-type specific responses by elucidating the molecular mechanisms of cGAMP import.

SLC46A2 is the third human cGAMP transporter we identified after SLC19A1, a minor importer in CD14^{+} monocytes, and the LRRC8 channels, which are used by primary endothelial cells (Lahey et al., 2020) (**Figure 7E**). We hypothesize that different cell types in the tumor microenvironment express different levels of these and other cGAMP transporters. Furthermore, surface levels of these transporters may also change as the cells respond to cGAMP and differentiate. Since different transporters have different affinities and kinetics toward extracellular cGAMP, it is likely that both the local concentrations of extracellular cGAMP and the orchestration of transporter expression dictate which set of cells in the tumor microenvironment respond to this immunotransmitter, and to what extent. For example, moderate concentrations of extracellular cGAMP might result in selective cGAMP import into IFN-I producing responder cells to promote immunity, whereas at higher concentrations, cGAMP could also be imported to responder cells that die from cGAMP to prevent hyperinflammation. Although mouse macrophages do not express Slc46a2, selective cGAMP uptake through differential expression of cGAMP importers may be a universal mechanism shared between humans and mice.

The cell-type specific responses to extracellular cGAMP and other CDNs indicate that CDN-based therapeutics would be most effective when targeting the correct cell types to

maximize the antitumoral immune response. Given that M1 macrophages produce high IFN-I levels in response to extracellular cGAMP signaling, optimizing therapeutics to specifically target their transporter SLC46A2 may result in more effective anticancer therapeutics. However, the species-specific usage of transporters tells a cautionary tale of testing CDN-based STING agonists in mice, despite mouse STING largely behaving similarly towards 2'3'-CDNs as human STING.

Beyond the role of the STING pathway in anti-cancer immunity, it has previously been shown in a murine model of colitis that commensal bacteria promote STING activation and inflammation partially independent of cGAS, suggesting that host cells are able to import and respond to bacterial-synthesized CDNs (Ahn et al., 2017). The bacterial CDNs 3'3'-cGAMP and 3'3'-CDA are associated with pathogenic bacteria (Corrigan et al., 2011; Davies et al., 2012; Woodward et al., 2010), while 3'3'-CDG is produced by a wide variety of bacteria, including commensals (Ryan et al., 2006). The ability of SLC46A2 and other CDN transporters (Lahey et al., 2020; Ritchie et al., 2019) to selectively import certain CDNs (such as cGAMP and 3'3'-CDA) but not others (3'3'-CDG) suggests that CDN transporters could regulate how the immune system differentially responds to pathogenic and commensal bacteria.

Acknowledgements
We thank all Li Lab members for their constructive comments and discussion through the course of this study. A.F.C. was supported by NIH 2T32GM007365. C.R. was supported by NIH 5T32GM007276. R.E.M. was supported by NSF GRFP 1656518. This work was supported by NIH grant DP2CA228044 (L.L). Cell sorting/flow cytometry analysis for this project was done on instruments in the Stanford Shared FACS Facility.

Author Contributions
A.F.C, C.R., V.B., and L.L. designed the study. A.F.C, C.R., R.E.M, and V.B. performed experiments. A.F.C, C.R., and L.L. wrote the manuscript. All authors discussed the findings and commented on the manuscript.

Competing interests
The authors declare no competing financial interests.

Data and materials availability
All data are available in the main text or the supplementary materials.

Figure Legends
Figure 1. Tumor-derived extracellular cGAMP alters the immune composition of 4T1 murine mammary tumors.
(A) BALB/c mice were injected with 50,000 4T1-Luciferase cells into the mammary fat pad. Once the tumors reached 100 mm^3, the tumors were irradiated with 0, 12, or 20 Gy. After 24 h, the mice were euthanized and the tumors were extracted and placed in cell culture media containing 50 μM STF-1084. The tumors incubated for 24 h, and then cGAMP was measured in the supernatants using cGAMP-Luc. n = 3 tumors for 0 Gy, n = 3 for 12 Gy, and n = 4 for 20 Gy. Data is shown as the mean ± SD.
(B) Experimental overview. BALB/c mice were injected with 50,000 4T1-Luciferase cells into the mammary fat pad. Once the tumors reached 100 mm^3, the tumors were irradiated with 0, 12, or 20 Gy. After 24 h, the tumors were injected with non-binding (NB) or neutralizing (Neu) STING. The mice were euthanized 24 h later and the tumors were extracted and prepared for flow cytometry.
(C-G) Mice were included from 3 independent experiments as outlined in (B). Outliers were excluded using the ROUT method, and any tumors that were identified as outliers were

removed from all analyses. n = 5 tumors for 0 Gy NB STING, n = 4 for 0 Gy Neu STING (1 outlier removed), n = 12 for 12 Gy NB STING (1 outlier removed), n = 10 for 12 Gy Neu STING (2 outliers removed), n = 11 for 20 Gy NB STING (1 outlier removed), and n = 12 for 20 Gy Neu STING. Data is shown as the mean ± SD. p values were calculated by unpaired t test with Welch's correction.
(C) $CD45^+$ immune cells as a percentage of all live cells.
(D) Representative flow cytometry plots identifying the $CD3^+$ populations in tumors from the 20 Gy NB and Neu STING groups.
(E) $CD3^+$ T cells as a percentage of all live cells.
(F) Live cells as a percentage of $CD3^+$ T cells (the upstream live/dead gate was omitted for this analysis).
(G) $F4/80^+$ macrophages as a percentage of all live cells.
(H) Table displaying each cell population as a percentage of all live cells in the 20 Gy groups. Significant changes ($p < 0.05$) are bolded.

Figure 2. Intratumoral $CD4^+$ T cells are direct responders to tumor-derived extracellular cGAMP.
(A-F) These data are from a subset of the experiments presented in Fig. 1 (C-G). Both the non-binding STING (NB) and neutralizing STING (Neu) groups received 12 Gy of radiation. Data is shown as the mean ± SD. p values were calculated by unpaired t test with Welch's correction.
(A) Representative flow cytometry plots identifying the $pSTING^+$ populations as a percentage of $CD3^+$ T cells in tumors from NB and Neu STING groups.
(B) $pSTING^+$ cells as a percentage of $CD3^+$ T cells.
(C) Representative flow cytometry plots identifying the $pIRF3^+$ populations as a percentage of $CD3^+$ T cells in tumors from NB and Neu STING groups.
(D) $pIRF3^+$ cells as a percentage of $CD3^+$ T cells.
(E) $pSTING^+$, $pIRF3^+$, $IFN\alpha^+$, and $IFN\beta^+$ cells as a percentage of $CD4^+$ T cells.
(F) $pSTING^+$, $pIRF3^+$, $IFN\alpha^+$, and $IFN\beta^+$ cells as a percentage of $CD8^+$ T cells.

Figure 3. Intratumoral $CD206^{Low}$ macrophages and Ly-$6C^+$ monocyte-lineage cells directly respond to tumor-derived extracellular cGAMP.
(A-G) These data are from a subset of the experiments presented in Fig. 1 (C-G). Both the non-binding STING (NB) and neutralizing STING (Neu) groups received 12 Gy of radiation. Data is shown as the mean ± SD. p values were calculated by unpaired t test with Welch's correction.
(A) Representative flow cytometry plots identifying the $pSTING^+$ populations as a percentage of $F4/80^+$ macrophages in tumors from NB and Neu STING groups.
(B) $pSTING^+$ cells as a percentage of $F4/80^+$ macrophages.
(C) $pSTING^+$ cells as a percentage of $F4/80^+/CD206^{Low}$ macrophages.
(D) $pIRF3^+$ cells as a percentage of $F4/80^+/CD206^{Low}$ macrophages.
(E) Geometric mean of IFNα (left) and IFNβ (right) in $F4/80^+/CD206^{Low}$ macrophages
(F) $CD206^{Low}$ cells as a percentage of $F4/80^+$ macrophages.
(G) $pSTING^+$ (left) and $pIRF3^+$ (right) cells as a percentage of Ly-$6C^+$ cells.

Figure 4. Intratumoral $NKG2D^{Low}$ NK cells directly respond to tumor-derived extracellular cGAMP.
(A-F) These data are from a subset of the experiments presented in Fig. 1 (C-G). Both the non-binding STING (NB) and neutralizing STING (Neu) groups received 12 Gy of radiation. Data is shown as the mean ± SD. p values were calculated by unpaired t test with Welch's correction.
(A) Representative flow cytometry plots identifying the $pSTING^+$ populations as a percentage of $CD335^+$ NK cells in tumors from NB and Neu STING groups.
(B) $pSTING^+$ cells as a percentage of $CD335^+$ NK cells.

(C) Geometric mean of IFNα (left) and IFNβ (right) in $CD335^+$ NK cells.
(D) $pSTING^+$ cells as a percentage of $CD335^+/NKG2D^{Low}$ NK cells
(E) $pIRF3^+$ cells as a percentage of $CD335^+/NKG2D^{Low}$ NK cells.
(F) $NKG2D^{Low}$ cells as a percentage of $CD335^+$ NK cells.
(G) Summary of the immune response to tumor-derived extracellular cGAMP.

Figure 5. Both human and mouse SLC46A2 are cGAMP transporters.
(A) Effect of sulfasalazine (SSZ) and methotrexate (MTX) on extracellular cGAMP signaling in $CD14^+$ monocytes. Cells were treated with 50 μM cGAMP for 2 h following a 15 min pretreatment with 1 mM SSZ or 500 μM MTX. (n = 3 individual donors.)
(B) Cartoon illustrating effects of the SLC19A1 inhibitors SSZ and MTX on extracellular cGAMP signaling in U937 cells compared to $CD14^+$ monocytes.
(C) Microarray RNA expression levels of genes annotated as plasma membrane, transmembrane transporters in U937 cells compared to $CD14^+$ monocytes.
(D) Effect of SLC46A2 overexpression on extracellular cGAMP signaling. U937-tet-SLC46A2-FLAG cells were induced with 1 μg/mL doxycycline (dox) for 24 h, then treated with 50 μM cGAMP. (n = 9 biological replicates.)
(E) Cartoon illustrating how cGAMP electroporation bypasses cGAMP transporters.
(F) Effect of SLC46A2 overexpression on intracellular cGAMP signaling. U937-tet-SLC46A2-FLAG cells were induced with 1 μg/mL dox for 24 h then electroporated with 100 nM cGAMP. (n = 2 biological replicates.)
(G) Effect of mouse Slc46a2 on extracellular cGAMP signaling. U937-tet-mSlc46a2-FLAG cells were induced with 1 μg/mL dox for 24 h then treated with 50 μM cGAMP. (n = 4 biological replicates.)
(H) Effect of mouse Slc46a2 on intracellular cGAMP signaling. U937-tet-mSlc46a2-FLAG cells were induced with 1 μg/mL dox for 24 h then electroporated with 100 nM cGAMP. (n = 1 biological replicate.)
For (A), (D), (F-H) data are shown as mean ± SD. See also Figure S6.

Figure 6. SLC46A2 transports synthetic and bacterial CDNs with varying selectivity.
(A-E) Effect of SLC46A2 on extracellular signaling of other CDNs. U937-tet-SLC46A2-FLAG cells were induced with 1 μg/mL dox for 24 h before treatment with either (A) 15 μM 2'3'-cG^SA^SMP, (B) 15 μM 2'3'-CDA^S, (C) 200 μM 3'3'-cGAMP, (D) 200 μM 3'3'-CDA, or (E) 200 μM 3'3'-CDG. (n = 2-3 biological replicates)
Data are shown as mean ± SD.

Figure 7. SLC46A2 is the dominant cGAMP importer in $CD14^+$ monocytes and monocyte-derived M1 macrophages.
(A) Effect of SSZ on SLC46A2 mediated cGAMP signaling. U937-tet-SLC46A2-FLAG cells were induced with 1 μg/mL dox for 24 h, then pretreated with 1 mM SSZ for 15 min before treatment with 50 μM cGAMP. (n = 4 biological replicates.) Data are shown as mean ± SD.
(B) Dose dependent inhibition of SSZ on SLC46A2 compared to $CD14^+$ monocytes. $CD14^+$ monocytes and induced U937-tet-SLC46A2-FLAG cells were pretreated with 30-2000 μM SSZ for 15 min before treatment with 50 μM cGAMP. Signal of pIRF3/tubulin was quantified by Western blot. Signal in uninduced cells was subtracted from induced cells to get SLC46A2 specific signal.
(C) Effect of partial CRISPR/Cas9 mediated knockout of SLC46A2 on extracellular cGAMP response in $CD14^+$ monocytes. Freshly isolated $CD14^+$ monocytes were electroporated with Cas9-sgRNA RNPs targeting SLC46A2. 3 d after electroporation, cells were treated with 50 μM cGAMP for 2 h. Signal of pIRF3 was quantified by Western blot, and the percentage of unedited, intact *SLC46A2* gene was estimated by ICE analysis of bulk sequencing.

(D) Role of SLC46A2 in $CD14^+$ monocyte derived cells. Monocyte derived M1 macrophages, M2 macrophages, and dendritic cells were treated with 50 μM cGAMP in the presence of either 1 mM SSZ or 500 μM MTX. (n = 1 individual donor.)
(E) Cartoon illustrating different potential cGAMP responder cell types in human tumors and their corresponding cGAMP transporters.
also Figure S7.

Figure S1. Gating scheme for flow cytometry analysis of tumors, related to Figure 1.
Immune cells were identified by CD45, and then further divided into immune subsets. T cells were identified by CD3, and then further divided into $CD4^+$ and $CD8^+$ T cells. B cells were identified by CD19, and dendritic cells were identified by CD11c. Monocyte lineage cells were identified by Ly-6C. Macrophages were identified by F4/80, and then further divided into $CD206^{Low}$ and $CD206^{High}$ subsets. NK cells were identified by CD335, and then further divided into $NKG2D^{Low}$ and $NKG2D^{High}$. Gates were drawn by identifying clear populations or by comparing the experimental samples to unstained controls.

Figure S2. Tumor-derived extracellular cGAMP alters the immune composition of 4T1 murine mammary tumors, related to Figure 1.
(A-H) Data is shown as the mean ± SD. p values were calculated by unpaired t test with Welch's correction.
(A) Live cells as a percentage of all singlets (left and right show different tests of significance).
(B) $CD4^+$ T cells as a percentage of all live cells.
(C) $CD8^+$ T cells as a percentage of all live cells.
(D) $CD4^+$ T cells as a percentage of $CD3^+$ T cells.
(E) $CD11c^+$ dendritic cells as a percentage of all live cells.
(F) $CD19^+$ B cells as a percentage of all live cells.
(G) $CD335^+$ T cells as a percentage of all live cells.
(H) Ly-$6C^+$ monocytic cells as a percentage of all live cells. Only a subset of the tumors was stained with this marker, so data is not available for 0 and 20 Gy.

Figure S3. Intratumoral $CD4^+$ T cells directly respond to tumor-derived extracellular cGAMP, related to Figure 2.
Both the non-binding STING (NB) and neutralizing STING (Neu) groups received 12 Gy of radiation. Data is shown as the mean ± SD. p values were calculated by unpaired t test with Welch's correction. $IFN\alpha^+$ (left) and $IFN\beta^+$ (right) cells as a percentage of $CD3^+$ T cells. Data is shown as the mean ± SD. p values were calculated by unpaired t test with Welch's correction**.**

Figure S4. Intratumoral macrophages and monocytic cells directly respond to tumor-derived extracellular cGAMP, related to Figure 3.
(A-I) Both the non-binding STING (NB) and neutralizing STING (Neu) groups received 12 Gy of radiation. Data is shown as the mean ± SD. p values were calculated by unpaired t test with Welch's correction.
(A) $pIRF3^+$ cells as a percentage of $F4/80^+$ macrophages.
(B) Geometric mean of IFNα (left) and IFNβ (right) in $F4/80^+$ macrophages.
(C) $pSTING^+$ cells as a percentage of $F4/80^+/CD206^{High}$ macrophages.
(D) $pIRF3^+$ cells as a percentage of $F4/80^+/CD206^{High}$ macrophages.
(E) Geometric mean of IFNα (left) and IFNβ (right) in $F4/80^+/CD206^{High}$ macrophages.
(F) $F4/80^+/CD206^{Low}$ macrophages as a percentage of all live cells.
(G) $F4/80^+/CD206^{High}$ macrophages as a percentage of all live cells.
(H) Representative flow cytometry plots identifying the $pSTING^+$ populations as a percentage of Ly-$6C^+$ cells in tumors from NB and Neu STING groups.

(I) IFNα$^+$ (left) and IFNβ$^+$ (right) cells as a percentage of Ly-6C$^+$ cells.

Figure S5. Intratumoral NK cells directly respond to tumor-derived extracellular cGAMP, while dendritic cells and B cells do not, related to Fig 4.
(A-G) Both the non-binding STING (NB) and neutralizing STING (Neu) groups received 12 Gy of radiation. Data is shown as the mean ± SD. p values were calculated by unpaired t test with Welch's correction.
(A) pIRF3$^+$ cells as a percentage of CD335$^+$ NK cells.
(B) pSTING$^+$ cells (left) and pIRF3$^+$ cells (right) as a percentage of CD335$^+$/NKG2D^{High} NK cells.
(C) Geometric mean of IFNα (left) and IFNβ (right) in CD335$^+$/NKG2D^{Low} NK cells.
(D) Geometric mean of IFNα (left) and IFNβ (right) in CD335$^+$/NKG2D^{High} NK cells.
(E) CD335$^+$/NKG2D^{Low} (left) and CD335$^+$/NKG2D^{High} (right) NK cells as a percentage of all live cells.
(F) pSTING$^+$ cells (left) and pIRF3$^+$ cells (right) as a percentage of CD11c$^+$ dendritic cells.
(G) pSTING$^+$, pIRF3$^+$, IFNα$^+$, and IFNβ$^+$ cells as a percentage of CD19$^+$ B cells.

Figure S6. Both human and mouse SLC46A2 are cGAMP transporters, related to Figure 5.
(A) Effect of mouse Slc19a1 on extracellular cGAMP signaling. U937-tet-mSlc19a1-FLAG cells were induced with 1 μg/mL dox for 24 h, then treated with 50 μM cGAMP. (n = 3 biological replicates.) Data are shown as mean ± SD.

Figure S7. SLC46A2 is the dominant cGAMP importer in CD14$^+$ monocytes and monocyte-derived M1 macrophages, related to Figure 7.
(A-C) Effects of the SLC19A1 inhibitors MTX, reduced folic acid (RFA), and oxidized folic acid (OFA) on SLC46A2 mediated cGAMP signaling. U937-tet-SLC46A2-FLAG cells were induced with 1 μg/mL dox for 24 h, then treated with 50 μM cGAMP in the presence of 500 μM of (A) MTX, (B) RFA, or (C) OFA for 2 h. (n = 2-3 biological replicates.)
(D) Effects of the SSZ metabolites 5-aminosalicylic acid (5-ASA) and sulfapyridine (SP) on SLC46A2 mediated cGAMP signaling. U937-tet-SLC46A2-FLAG cells were induced with 1 μg/mL dox for 24 h, then pretreated with 1 mM 5-ASA or SP for 15 min before treatment with 50 μM cGAMP for 2 h. (n = 2 biological replicates.)
(E) Effect of SLC19A1 inhibitors on mouse Slc46a2 mediated cGAMP signaling. U937-tet-mSlc46a2-FLAG cells were induced with 1 μg/mL dox for 24 h, then treated with 50 μM cGAMP in the presence of 1 mM SSZ or 500 μM MTX, RFA, or OFA. Data are shown as mean ± SD. (n = 2 biological replicates.)
(F-G) RNA-seq expression of SLC46A2 homologs in select (F) human and (G) mouse immune cells from Immgen.
(H) BALB/c mice were injected with 50,000 4T1-Luciferase cells into the mammary fat pad. Once the tumors reached 100 mm^3, the tumors were irradiated with 12 Gy. After 24 h, the tumors were injected with non-binding STING. The mice were euthanized 24 h later and the tumors were extracted and prepared for FACS. 2-3 tumors were pooled into individual samples in order to increase the number of target cells. Cells were sorted into CD206^{High} and CD206^{Low} macrophages according to a gating scheme similar to Figure S1 and then submitted for RNA-seq analysis. Expression values are displayed as transcripts per million (TPM). Data is presented as the mean of two samples per cell type, with the SD in parentheses.
For (A-E) data are shown as mean ± SD.

Methods

Cell Culture

HEK 293T cells used for lentivirus generation were maintained in DMEM (Cellgro) supplemented with 10% FBS (Atlanta Biologicals) and 1% penicillin-streptomycin (GIBCO).

U937 and $CD14^+$ cells were maintained in RPMI (Cellgro) supplemented with 10% heat-inactivated FBS (Atlanta Biologicals) and 1% penicillin-streptomycin (GIBCO). 4T1-luciferase cells were a gift from Dr. Edward Graves (Vilalta et al., 2014) and were maintained in RPMI (Cellgro) supplemented with 10% heat-inactivated FBS (Atlanta Biologicals) and 1% penicillin-streptomycin (GIBCO). All cells were maintained in a 5% CO_2 incubator at 37 °C.

Recombinant DNA

A plasmid containing the CDS of human SLC46A2 (pCMV-SPORT6-SLC46A2) was purchased from Harvard Plasmid Database. Custom plasmids (pTwist-CMV) containing the CDSs of mouse Slc19a1 and Slc46a2 were purchased from Twist Bioscience. To generate doxycycline inducible lentiviral plasmids, the transporter CDS was amplified from the appropriate plasmid using the primers listed in Supplemental Table 1 and cloned into EcoRI/BamHI linearized pLVX-TetOne-FLAG-Hydro plasmid (Lahey et al., 2020) by isothermal Gibson assembly (Gibson et al., 2009).

Mouse Models

7-9 week-old female BALB/c mice (Jackson Laboratories) were inoculated with 5 x 10^4 4T1-luciferase cells suspended in 50 µL of PBS. The cells were injected into the right fifth mammary fat pad. When tumor volume reached 100 ± 20 mm^3, tumors were irradiated with 0, 12, or 20 Gy using a 225 kVp cabinet X-ray irradiator with a 0.5 mm Cu filter (IC-250, Kimtron Inc.). Mice were anesthetized with a mixture of 80 mg/kg ketamine (VetaKet) and 5 mg/kg xylazine (AnaSed) prior to irradiation and were shielded with a 3.2 mm lead shield with 15 x 20 mm apertures to expose the tumors. For the 0 Gy treatment, mice were anesthetized but not irradiated.

For the detection of tumor-derived extracellular cGAMP, mice were euthanized 24 h after irradiation. Tumors were weighed and then cut into smaller pieces before being placed into tissue culture plates with 1 mL of RPMI supplemented with 10% heat-inactivated FBS and 1% penicillin-streptomycin, as well as 50 µM STF-1084 (Carozza et al., 2020). Tumors were incubated at 37°C for 24 h and then the supernatants were collected for cGAMP quantification.

For flow cytometry, mice were intratumorally injected with 100 µL of 100 µM neutralizing STING or non-binding STING 24 h after irradiation. Mice were euthanized 24 h later and the tumors were extracted.

Mice were maintained at Stanford University in compliance with the Stanford University Institutional Animal Care and Use Committee (IACUC) regulations. All procedures were approved by the Stanford University Administrative Panel on Laboratory Animal Care (APLAC).

cGAMP Quantification

Tumor-derived extracellular cGAMP was quantified using STING-CAP and cGAMP-Luc (Mardjuki et al., 2020). In brief, cGAMP was extracted from the tumor supernatants by binding it to His-tagged STING, which was then collected by magnetic nickel beads. The beads were subsequently washed and boiled in a minimal volume of buffer to elute cGAMP. In cGAMP-Luc, cGAMP was first degraded by the enzyme ENPP1, converting cGAMP to AMP and GMP. AMP was enzymatically converted to ATP, which was then measured using a luciferase assay (CellTiter-Glo, Promega). The cGAMP concentrations were normalized by the weight of the tumor.

STING Expression and Purification

Wild-type (neutralizing) and R237A (non-binding) STING were expressed and purified using previously published methods (Carozza et al., 2020). In brief, pTB146 His-SUMO-mSTING (residues 139-378) was expressed in Rosetta (DE3)pLysS competent cells (Sigma-Aldrich). Cells were grown in 2xYT medium with 100 µg/mL ampicillin until they reached an OD600 of 1.

They were then induced with 0.75 mM IPTG at 16°C overnight. Cells were pelleted and resuspended in 50 mM Tris pH 7.5, 400 mM NaCl, 10 mM imidazole, 2 mM DTT, and protease inhibitors (cOmplete, EDTA-free protease inhibitor cocktail Roche). The cells were then flash frozen and thawed twice before sonication in order to lyse the cells. The lysate was then spun at 40,000 rpm at 4°C for 1 h. The supernatant was incubated with HisPur cobalt resin (Thermo Scientific) for 30 minutes at 4°C. The resin-bound protein was washed with 50 column volumes of 50 mM Tris pH 7.5, 150 mM NaCl, 2% triton X-114; 50 column volumes of 50 mM Tris pH 7.5, 1 M NaCl; and 20 column volumes of 50 mM Tris pH 7.5, 150 mM NaCl. Protein was eluted from resin with 600 mM imidazole in 50 mM Tris pH 7.5, 150 mM NaCl. Fractions containing His-SUMO-STING were pooled, concentrated, and dialyzed against 50 mM Tris pH 7.5, 150 mM NaCl while incubating with the SUMOlase His-ULP1 to remove the His-SUMO tag overnight. The solution was incubated with the HisPur cobalt resin again to remove the His-SUMO tag, and STING was collected from the flowthrough. Protein was dialyzed against 20 mM Tris pH 7.5, loaded onto a HitrapQ anion exchange column (GE Healthcare) using an Äkta FPLC (GE Healthcare), and eluted with a NaCl gradient. Fractions containing STING were pooled, buffer exchanged into PBS, and stored at -80°C until use.

Flow Cytometry Analysis of Tumors

Following tumor extraction, the tumors were incubated in 10 mL of RPMI supplemented with 10% heat-inactivated FBS and 1% penicillin-streptomycin, as well as 20 µg/mL DNase I type IV (Millipore) and 1 mg/mL collagenase from Clostridium histolyticum (Sigma-Aldrich), at 37°C for 30 min. The samples were then passed through a 100 µm cell strainer (Sigma-Aldrich) to form a single-cell suspension. Red blood cells were lysed in 155 mM NH_4Cl, 12 mM $NaHCO_3$, and 0.1 mM EDTA for 5 min at room temperature.

The samples designated for interferon detection were resuspended in 1 mL of RPMI supplemented with 10% heat-inactivated FBS and 1% penicillin-streptomycin and placed in a 5% CO_2 incubator at 37°C for 1 h. 5 µg/mL Brefeldin A (BioLegend) was added to each sample, and they were incubated at 37°C for 5 additional hours before proceeding. All other samples proceeded directly to the live/dead stain after the red blood cell lysis.

Samples were stained with LIVE/DEAD Fixable Blue Dead Cell Stain (Invitrogen) for 30 min. Samples were then fixed and permeabilized with either eBioscience Foxp3/Transcription Factor Staining Buffer Set (Invitrogen) or Fixation/Permeabilization Solution Kit (BD Biosciences). Samples were Fc-blocked for 10 min using TruStain fcX (BioLegend), and then stained for 1 h (see Supplemental Table 2 for antibodies and dilutions). All samples were run on an Aurora analyzer (Cytek).

FACS Sorting of Tumor Macrophages

BALB/c mice were injected with 50,000 4T1-Luciferase cells into the mammary fat pad. Once the tumors reached 100 mm^3, the tumors were irradiated with 12 Gy. After 24 h, the tumors were injected with non-binding STING. The mice were euthanized 24 h later and the tumors were extracted and prepared for FACS. 2-3 tumors were pooled into individual samples in order to increase the number of target cells. Following tumor extraction, the tumors were incubated in 10 mL of RPMI supplemented with 10% heat-inactivated FBS and 1% penicillin-streptomycin, as well as 20 µg/mL DNase I type IV (Millipore) and 1 mg/mL collagenase from Clostridium histolyticum (Sigma-Aldrich), at 37°C for 30 min. The samples were then passed through a 100 µm cell strainer (Sigma-Aldrich) to form a single-cell suspension. Red blood cells were lysed in 155 mM NH_4Cl, 12 mM $NaHCO_3$, and 0.1 mM EDTA for 5 min at room temperature. Samples were stained with LIVE/DEAD Fixable Blue Dead Cell Stain (Invitrogen) for 30 min, and then stained for 1 h (see tables for antibodies and dilutions). Cells were sorted into $CD206^{High}$ and $CD206^{Low}$ macrophages using a FACSAria II (BD) cell sorter. The gating scheme for the sort

was similar to the scheme presented in Supplementary Figure 1. The sorted samples were then spun down and resuspended in 1 mL Trizol (Invitrogen) before being sent for RNA-seq.

RNA-Seq

RNA-seq of tumor macrophages was performed by the Stanford Functional Genomics Facility. RNA was isolated using a guanidinium thiocyanate-phenol-chloroform extraction (TRIzol). Libraries were prepared using a Poly-A-enriched mRNA-Seq Library kit (KAPA) and were sequenced on a HiSeq 4000 (Illumina) using 2 x 75 bp paired-end reads. Demultiplexed reads were aligned to the GRCm38.p6 annotated mouse genome (GENCODE vM24) using STAR v2.7 in two-pass mode. Read counts for annotated genes were subsequently normalized to Transcripts Per Million (TPM) (Wagner et al., 2012).

Synthesis and purification of cGAMP

cGAMP was synthesized as previously described (Ritchie et al., 2019). To enzymatically synthesize cGAMP, 1 µM purified sscGAS was incubated with 50 mM Tris-HCl pH 7.4, 2 mM ATP, 2 mM GTP, 20 mM $MgCl_2$, and 100 µg/mL herring testis DNA (Sigma) for 24 h. The reaction was then heated at 95 °C for 3 min and filtered through a 3-kDa filter. cGAMP was purified from the reaction mixture using a PLRP-S polymeric reversed phase preparatory column (100 Å, 8 µm, 300 x 25 mm; Agilent Technologies) on a preparatory HPLC (1260 Infinity LC system; Agilent Technologies) connected to UV-vis detector (ProStar; Agilent Technologies) and fraction collector (440-LC; Agilent Technologies). The flow rate was set to 25 mL/min. The mobile phase consisted of 10 mM triethylammonium acetate in water and acetonitrile. The mobile phase started as 2% acetonitrile for first 5 min. Acetonitrile was then ramped up to 30% from 5-20 min, then to 90% from 20-22 min, maintained at 90% from 22-25 min, and then ramped down to 2% from 25-28 min. Fractions containing cGAMP were lyophilized and resuspended in water. The concentration was determined by measuring absorbance at 280 nm.

Generation of Doxycycline Inducible Cell Lines

Lentiviral packaging plasmids (pHDM-G, pHDM-Hgmp2, pHDM-tat1b, and RC/CMV-rev1b) were purchased from Harvard Medical School. To generate lentivirus, 500 ng of lentiviral plasmid encoding doxycycline inducible transporters and 500 ng of each of the packaging plasmids were transfected into HEK 293T cells with FuGENE 6 transfection reagent (Promega). Cell supernatant was replaced 24 h after transfection and harvested after another 24 h. The lentivirus containing supernatant was passed through a 0.45 µm filter. To create the U937 *SLC19A1*$^{-/-}$ cell line (Ritchie et al., 2019), 1 mL filtered supernatant was supplemented with 8 mg/mL polybrene (Sigma Aldrich) and added to 1 x 10^5 cells in a 24 well plate. Cells were spun at 1000 x g for 1 h, after which the virus containing media was removed and cells were resuspended in fresh media. After 48 h, cells were put under selection with the appropriate antibiotic alongside control cells (uninfected) until all control cells died.

CDN Stimulation

U937 cells (0.5 x 10^6 cells/mL) or freshly isolated CD14+ monocytes (1 x 10^6 cells/mL) were treated with the indicated concentration of CDN for 2 h in a 5% CO_2 incubator at 37 °C, unless otherwise indicated. Following treatments, cells were collected, lysed with Laemmli Sample Buffer, and run on SDS-PAGE gels for Western blot analysis.

Electroporation of CDNs

U937 cells were pelleted and resuspended in nucleofector solution (90 mM Na_2HPO_4, 90 mM NaH_2PO_4, 5 mM KCl, 10 mM $MgCl_2$, 10 mM sodium succinate) with the indicated CDN concentrations to a density of 1 x 10^6 cells/mL. 100 uL cells were then transferred to a 0.2 cm electroporation cuvette and electroporated with program U-013 on a Nucleofector IIb device.

Immediately after nucleofection, 500 uL media was added to cells. Cells were then transferred to a 24 well plate containing an additional 900 uL media and incubated in a 5% CO2 incubator at 37 °C for 2 h. Following this, cells were collected, lysed with Laemmli Sample Buffer, and run on SDS-PAGE gels for Western blot analysis.

Analysis of Microarray Data

Microarray data of RNA transcript expression levels in U937 cells and $CD14^+$ monocytes from three donors was retrieved from Gene Expression Omnibus, accession GSE16076 (Gebhard et al., 2010). For each microarray, background signal was subtracted from all probes so that the probe with the least signal was set to zero. Expression of transcripts in $CD14^+$ monocytes was averaged across the three donors. Microarray probes targeting genes that were annotated in GeneOntology (accessed on 02-23-2020) as both transmembrane transporters (GO:0055085) and localized to plasma membrane (GO:0005886) were isolated to look for differential expression of transporters between U937 cells and CD14+ monocytes.

Isolation of $CD14^+$ Monocytes

Buffy coat (Stanford Blood Center) was diluted 1:3 with PBS supplemented with 2 mM EDTA. Diluted buffy coat was layered on top of 50% Percoll (GE Healthcare) containing 140 mM NaCl and centrifuged at 600 x g for 30 min. The separated PBMC layer was collected and washed once with PBS and once with RPMI. Following this, $CD14^+$ cells were labeled using CD14 MicroBeads (Miltenyi Biotec) and isolated using a MACS LS Column on a MidiMACS Separator (Miltenyi Biotec) following the manufacturer's instructions.

Differentiation of $CD14^+$ Monocytes

Freshly isolated $CD14^+$ monocytes were differentiated into either M1 macrophages, M2 macrophages, or dendritic cells using a previously-described phased protocol (Zarif et al., 2016). In all three differentiation cases, $CD14^+$ monocytes are seeded to a density of 3×10^5 cells/mL in fresh RPMI media containing 10% heat-inactivated FBS and 1% penicillin-streptomycin on day 0; media was replaced on day 5; and a CDN stimulation experiment was performed on day 9. To differentiate into M1 macrophages, media was supplemented with 20 ng/mL GM-CSF on day 0, then supplemented with 20 ng/mL GM-CSF (PeproTech), 20 ng/mL IFN-γ (PeproTech), 20 ng/mL IL-5 (PeproTech), and 20 ng/mL LPS on day 5. To differentiate into M2 macrophages, media was supplemented with 20 ng/mL M-CSF (PeproTech) on day 0, then supplemented with 20 ng/mL M-CSF, 20 ng/mL IL-4, 20 ng/mL IL-6 (PeproTech), and 20 ng/mL IL-13 (PeproTech) on day 5. To differentiate into dendritic cells, media was supplemented with 100 ng/mL GM-CSF and 20 ng/mL IL-4 on both day 0 and day 5.

References

Ablasser, A., Goldeck, M., Cavlar, T., Deimling, T., Witte, G., Rohl, I., Hopfner, K.P., Ludwig, J., and Hornung, V. (2013a). cGAS produces a 2'-5'-linked cyclic dinucleotide second messenger that activates STING. Nature *498*, 380-384.

Ablasser, A., Schmid-Burgk, J.L., Hemmerling, I., Horvath, G.L., Schmidt, T., Latz, E., and Hornung, V. (2013b). Cell intrinsic immunity spreads to bystander cells via the intercellular transfer of cGAMP. Nature *503*, 530-534.

Ahn, J., Son, S., Oliveira, S.C., and Barber, G.N. (2017). STING-Dependent Signaling Underlies IL-10 Controlled Inflammatory Colitis. Cell Rep *21*, 3873-3884.

Andzinski, L., Spanier, J., Kasnitz, N., Kroger, A., Jin, L., Brinkmann, M.M., Kalinke, U., Weiss, S., Jablonska, J., and Lienenklaus, S. (2016). Growing tumors induce a local STING dependent Type I IFN response in dendritic cells. Int J Cancer *139*, 1350-1357.

Bakhoum, S.F., and Cantley, L.C. (2018). The Multifaceted Role of Chromosomal Instability in Cancer and Its Microenvironment. Cell *174*, 1347-1360.

Bakhoum, S.F., Ngo, B., Laughney, A.M., Cavallo, J.A., Murphy, C.J., Ly, P., Shah, P., Sriram, R.K., Watkins, T.B.K., Taunk, N.K., *et al.* (2018). Chromosomal instability drives metastasis through a cytosolic DNA response. Nature *553*, 467-472.
Blank, C., Brown, I., Peterson, A.C., Spiotto, M., Iwai, Y., Honjo, T., and Gajewski, T.F. (2004). PD-L1/B7H-1 inhibits the effector phase of tumor rejection by T cell receptor (TCR) transgenic CD8+ T cells. Cancer Res *64*, 1140-1145.
Carozza, J.A., Böhnert, V., Nguyen, K.C., Skariah, G., Shaw, K.E., Brown, J.A., Rafat, M., von Eyben, R., Graves, E.E., Glenn, J.S., *et al.* (2020). Extracellular cGAMP is a cancer-cell-produced immunotransmitter involved in radiation-induced anticancer immunity. Nat Cancer *1*, 184-196.
Cerboni, S., Jeremiah, N., Gentili, M., Gehrmann, U., Conrad, C., Stolzenberg, M.C., Picard, C., Neven, B., Fischer, A., Amigorena, S., *et al.* (2017). Intrinsic antiproliferative activity of the innate sensor STING in T lymphocytes. J Exp Med *214*, 1769-1785.
Cheng, N., Watkins-Schulz, R., Junkins, R.D., David, C.N., Johnson, B.M., Montgomery, S.A., Peine, K.J., Darr, D.B., Yuan, H., McKinnon, K.P., *et al.* (2018). A nanoparticle-incorporated STING activator enhances antitumor immunity in PD-L1-insensitive models of triple-negative breast cancer. JCI Insight *3*.
Corrales, L., Glickman, L.H., McWhirter, S.M., Kanne, D.B., Sivick, K.E., Katibah, G.E., Woo, S.R., Lemmens, E., Banda, T., Leong, J.J., *et al.* (2015). Direct Activation of STING in the Tumor Microenvironment Leads to Potent and Systemic Tumor Regression and Immunity. Cell Rep *11*, 1018-1030.
Corrigan, R.M., Abbott, J.C., Burhenne, H., Kaever, V., and Grundling, A. (2011). c-di-AMP is a new second messenger in Staphylococcus aureus with a role in controlling cell size and envelope stress. PLoS Pathog *7*, e1002217.
Curran, E., Chen, X., Corrales, L., Kline, D.E., Dubensky, T.W., Jr., Duttagupta, P., Kortylewski, M., and Kline, J. (2016). STING Pathway Activation Stimulates Potent Immunity against Acute Myeloid Leukemia. Cell Rep *15*, 2357-2366.
Davies, B.W., Bogard, R.W., Young, T.S., and Mekalanos, J.J. (2012). Coordinated regulation of accessory genetic elements produces cyclic di-nucleotides for V. cholerae virulence. Cell *149*, 358-370.
Demaria, O., De Gassart, A., Coso, S., Gestermann, N., Di Domizio, J., Flatz, L., Gaide, O., Michielin, O., Hwu, P., Petrova, T.V., *et al.* (2015). STING activation of tumor endothelial cells initiates spontaneous and therapeutic antitumor immunity. Proc Natl Acad Sci U S A *112*, 15408-15413.
Deng, L., Liang, H., Xu, M., Yang, X., Burnette, B., Arina, A., Li, X.D., Mauceri, H., Beckett, M., Darga, T., *et al.* (2014). STING-Dependent Cytosolic DNA Sensing Promotes Radiation-Induced Type I Interferon-Dependent Antitumor Immunity in Immunogenic Tumors. Immunity *41*, 843-852.
Downey, C.M., Aghaei, M., Schwendener, R.A., and Jirik, F.R. (2014). DMXAA causes tumor site-specific vascular disruption in murine non-small cell lung cancer, and like the endogenous non-canonical cyclic dinucleotide STING agonist, 2'3'-cGAMP, induces M2 macrophage repolarization. PLoS One *9*, e99988.
Gaidt, M.M., Ebert, T.S., Chauhan, D., Ramshorn, K., Pinci, F., Zuber, S., O'Duill, F., Schmid-Burgk, J.L., Hoss, F., Buhmann, R., *et al.* (2017). The DNA Inflammasome in Human Myeloid Cells Is Initiated by a STING-Cell Death Program Upstream of NLRP3. Cell *171*, 1110-1124 e1118.
Gao, P., Ascano, M., Wu, Y., Barchet, W., Gaffney, B.L., Zillinger, T., Serganov, A.A., Liu, Y., Jones, R.A., Hartmann, G., *et al.* (2013). Cyclic [G(2',5')pA(3',5')p] is the metazoan second messenger produced by DNA-activated cyclic GMP-AMP synthase. Cell *153*, 1094-1107.
Gebhard, C., Benner, C., Ehrich, M., Schwarzfischer, L., Schilling, E., Klug, M., Dietmaier, W., Thiede, C., Holler, E., Andreesen, R., *et al.* (2010). General transcription factor binding at CpG

islands in normal cells correlates with resistance to de novo DNA methylation in cancer cells. Cancer Res *70*, 1398-1407.
Gibson, D.G., Young, L., Chuang, R.Y., Venter, J.C., Hutchison, C.A., 3rd, and Smith, H.O. (2009). Enzymatic assembly of DNA molecules up to several hundred kilobases. Nat Methods *6*, 343-345.
Gilfillan, S., Ho, E.L., Cella, M., Yokoyama, W.M., and Colonna, M. (2002). NKG2D recruits two distinct adapters to trigger NK cell activation and costimulation. Nat Immunol *3*, 1150-1155.
Gulen, M.F., Koch, U., Haag, S.M., Schuler, F., Apetoh, L., Villunger, A., Radtke, F., and Ablasser, A. (2017). Signalling strength determines proapoptotic functions of STING. Nat Commun *8*, 427.
Harding, S.M., Benci, J.L., Irianto, J., Discher, D.E., Minn, A.J., and Greenberg, R.A. (2017). Mitotic progression following DNA damage enables pattern recognition within micronuclei. Nature *548*, 466-470.
Huntington, N.D., Vosshenrich, C.A., and Di Santo, J.P. (2007). Developmental pathways that generate natural-killer-cell diversity in mice and humans. Nat Rev Immunol *7*, 703-714.
Ishikawa, H., Ma, Z., and Barber, G.N. (2009). STING regulates intracellular DNA-mediated, type I interferon-dependent innate immunity. Nature *461*, 788-792.
Iwai, Y., Ishida, M., Tanaka, Y., Okazaki, T., Honjo, T., and Minato, N. (2002). Involvement of PD-L1 on tumor cells in the escape from host immune system and tumor immunotherapy by PD-L1 blockade. Proc Natl Acad Sci U S A *99*, 12293-12297.
Jutila, M.A., Kroese, F.G., Jutila, K.L., Stall, A.M., Fiering, S., Herzenberg, L.A., Berg, E.L., and Butcher, E.C. (1988). Ly-6C is a monocyte/macrophage and endothelial cell differentiation antigen regulated by interferon-gamma. Eur J Immunol *18*, 1819-1826.
Konno, H., Konno, K., and Barber, G.N. (2013). Cyclic dinucleotides trigger ULK1 (ATG1) phosphorylation of STING to prevent sustained innate immune signaling. Cell *155*, 688-698.
Kurahara, H., Shinchi, H., Mataki, Y., Maemura, K., Noma, H., Kubo, F., Sakoda, M., Ueno, S., Natsugoe, S., and Takao, S. (2011). Significance of M2-polarized tumor-associated macrophage in pancreatic cancer. J Surg Res *167*, e211-219.
Lahey, L.J., Wen, X., Mardjuki, R.E., Böhnert, V., Hess, G.T., Ritchie, C., Carozza, J.A., Maduke, M., Bassik, M.C., and Li, L. (2020). The LRRC8A:C Heteromeric Channel Is a cGAMP Transporter and the Dominant cGAMP Importer in Human Vasculature Cells. bioRxiv.
Larkin, B., Ilyukha, V., Sorokin, M., Buzdin, A., Vannier, E., and Poltorak, A. (2017). Cutting Edge: Activation of STING in T Cells Induces Type I IFN Responses and Cell Death. J Immunol *199*, 397-402.
Laursen, M.F., Christensen, E., Degn, L.L.T., Jonsson, K., Jakobsen, M.R., Agger, R., and Kofod-Olsen, E. (2018). CD11c-targeted Delivery of DNA to Dendritic Cells Leads to cGAS- and STING-dependent Maturation. J Immunother *41*, 9-18.
Leach, D.R., Krummel, M.F., and Allison, J.P. (1996). Enhancement of antitumor immunity by CTLA-4 blockade. Science *271*, 1734-1736.
Luteijn, R.D., Zaver, S.A., Gowen, B.G., Wyman, S.K., Garelis, N.E., Onia, L., McWhirter, S.M., Katibah, G.E., Corn, J.E., Woodward, J.J*., et al.* (2019). SLC19A1 transports immunoreactive cyclic dinucleotides. Nature *573*, 434-438.
Mackenzie, K.J., Carroll, P., Martin, C.A., Murina, O., Fluteau, A., Simpson, D.J., Olova, N., Sutcliffe, H., Rainger, J.K., Leitch, A*., et al.* (2017). cGAS surveillance of micronuclei links genome instability to innate immunity. Nature *548*, 461-465.
Marcus, A., Mao, A.J., Lensink-Vasan, M., Wang, L., Vance, R.E., and Raulet, D.H. (2018). Tumor-Derived cGAMP Triggers a STING-Mediated Interferon Response in Non-tumor Cells to Activate the NK Cell Response. Immunity *49*, 754-763 e754.
Mardjuki, R.E., Carozza, J.A., and Li, L. (2020). Development of cGAMP-Luc, a sensitive and precise coupled enzyme assay to measure cGAMP in complex biological samples. J Biol Chem.

Murray, P.J., Allen, J.E., Biswas, S.K., Fisher, E.A., Gilroy, D.W., Goerdt, S., Gordon, S., Hamilton, J.A., Ivashkiv, L.B., Lawrence, T.*, et al.* (2014). Macrophage activation and polarization: nomenclature and experimental guidelines. Immunity *41*, 14-20.
Nicolai, C.J., Wolf, N., Chang, I.C., Kirn, G., Marcus, A., Ndubaku, C.O., McWhirter, S.M., and Raulet, D.H. (2020). NK cells mediate clearance of CD8(+) T cell-resistant tumors in response to STING agonists. Sci Immunol *5*.
Ohkuri, T., Kosaka, A., Ishibashi, K., Kumai, T., Hirata, Y., Ohara, K., Nagato, T., Oikawa, K., Aoki, N., Harabuchi, Y.*, et al.* (2017). Intratumoral administration of cGAMP transiently accumulates potent macrophages for anti-tumor immunity at a mouse tumor site. Cancer Immunol Immunother *66*, 705-716.
Porcheray, F., Viaud, S., Rimaniol, A.C., Leone, C., Samah, B., Dereuddre-Bosquet, N., Dormont, D., and Gras, G. (2005). Macrophage activation switching: an asset for the resolution of inflammation. Clin Exp Immunol *142*, 481-489.
Ritchie, C., Cordova, A.F., Hess, G.T., Bassik, M.C., and Li, L. (2019). SLC19A1 Is an Importer of the Immunotransmitter cGAMP. Mol Cell *75*, 372-381.
Ryan, R.P., Fouhy, Y., Lucey, J.F., and Dow, J.M. (2006). Cyclic di-GMP signaling in bacteria: recent advances and new puzzles. J Bacteriol *188*, 8327-8334.
Sharma, P., and Allison, J.P. (2015). The future of immune checkpoint therapy. Science *348*, 56-61.
Shrikant, P., Khoruts, A., and Mescher, M.F. (1999). CTLA-4 blockade reverses CD8+ T cell tolerance to tumor by a CD4+ T cell- and IL-2-dependent mechanism. Immunity *11*, 483-493.
Sinha, P., Clements, V.K., and Ostrand-Rosenberg, S. (2005). Reduction of myeloid-derived suppressor cells and induction of M1 macrophages facilitate the rejection of established metastatic disease. J Immunol *174*, 636-645.
Sivick, K.E., Desbien, A.L., Glickman, L.H., Reiner, G.L., Corrales, L., Surh, N.H., Hudson, T.E., Vu, U.T., Francica, B.J., Banda, T.*, et al.* (2018). Magnitude of Therapeutic STING Activation Determines CD8(+) T Cell-Mediated Anti-tumor Immunity. Cell Rep *25*, 3074-3085 e3075.
Smedegard, G., and Bjork, J. (1995). Sulphasalazine: mechanism of action in rheumatoid arthritis. Br J Rheumatol *34 Suppl 2*, 7-15.
Steidl, C., Lee, T., Shah, S.P., Farinha, P., Han, G., Nayar, T., Delaney, A., Jones, S.J., Iqbal, J., Weisenburger, D.D.*, et al.* (2010). Tumor-associated macrophages and survival in classic Hodgkin's lymphoma. N Engl J Med *362*, 875-885.
Sun, L., Wu, J., Du, F., Chen, X., and Chen, Z.J. (2013). Cyclic GMP-AMP synthase is a cytosolic DNA sensor that activates the type I interferon pathway. Science *339*, 786-791.
Tang, C.H., Zundell, J.A., Ranatunga, S., Lin, C., Nefedova, Y., Del Valle, J.R., and Hu, C.C. (2016). Agonist-Mediated Activation of STING Induces Apoptosis in Malignant B Cells. Cancer Res *76*, 2137-2152.
Vilalta, M., Rafat, M., Giaccia, A.J., and Graves, E.E. (2014). Recruitment of circulating breast cancer cells is stimulated by radiotherapy. Cell Rep *8*, 402-409.
Wagner, G.P., Kin, K., and Lynch, V.J. (2012). Measurement of mRNA abundance using RNA-seq data: RPKM measure is inconsistent among samples. Theory Biosci *131*, 281-285.
Wang, J., Li, P., Yu, Y., Fu, Y., Jiang, H., Lu, M., Sun, Z., Jiang, S., Lu, L., and Wu, M.X. (2020). Pulmonary surfactant-biomimetic nanoparticles potentiate heterosubtypic influenza immunity. Science *367*.
Woodward, J.J., Iavarone, A.T., and Portnoy, D.A. (2010). c-di-AMP secreted by intracellular Listeria monocytogenes activates a host type I interferon response. Science *328*, 1703-1705.
Wu, J., Sun, L., Chen, X., Du, F., Shi, H., Chen, C., and Chen, Z.J. (2013). Cyclic GMP-AMP is an endogenous second messenger in innate immune signaling by cytosolic DNA. Science *339*, 826-830.

Xia, T., Konno, H., Ahn, J., and Barber, G.N. (2016). Deregulation of STING Signaling in Colorectal Carcinoma Constrains DNA Damage Responses and Correlates With Tumorigenesis. Cell Rep *14*, 282-297.

Zarif, J.C., Hernandez, J.R., Verdone, J.E., Campbell, S.P., Drake, C.G., and Pienta, K.J. (2016). A phased strategy to differentiate human CD14+monocytes into classically and alternatively activated macrophages and dendritic cells. Biotechniques *61*, 33-41.

Zhou, C., Chen, X., Planells-Cases, R., Chu, J., Wang, L., Cao, L., Li, Z., Lopez-Cayuqueno, K.I., Xie, Y., Ye, S.*, et al.* (2020a). Transfer of cGAMP into Bystander Cells via LRRC8 Volume-Regulated Anion Channels Augments STINGMediated Interferon Responses and Anti-viral Immunity. Immunity *52*, 1-15.

Zhou, Y., Fei, M., Zhang, G., Liang, W.C., Lin, W., Wu, Y., Piskol, R., Ridgway, J., McNamara, E., Huang, H.*, et al.* (2020b). Blockade of the Phagocytic Receptor MerTK on Tumor-Associated Macrophages Enhances P2X7R-Dependent STING Activation by Tumor-Derived cGAMP. Immunity *52*, 357-373 e359.

Figure 1

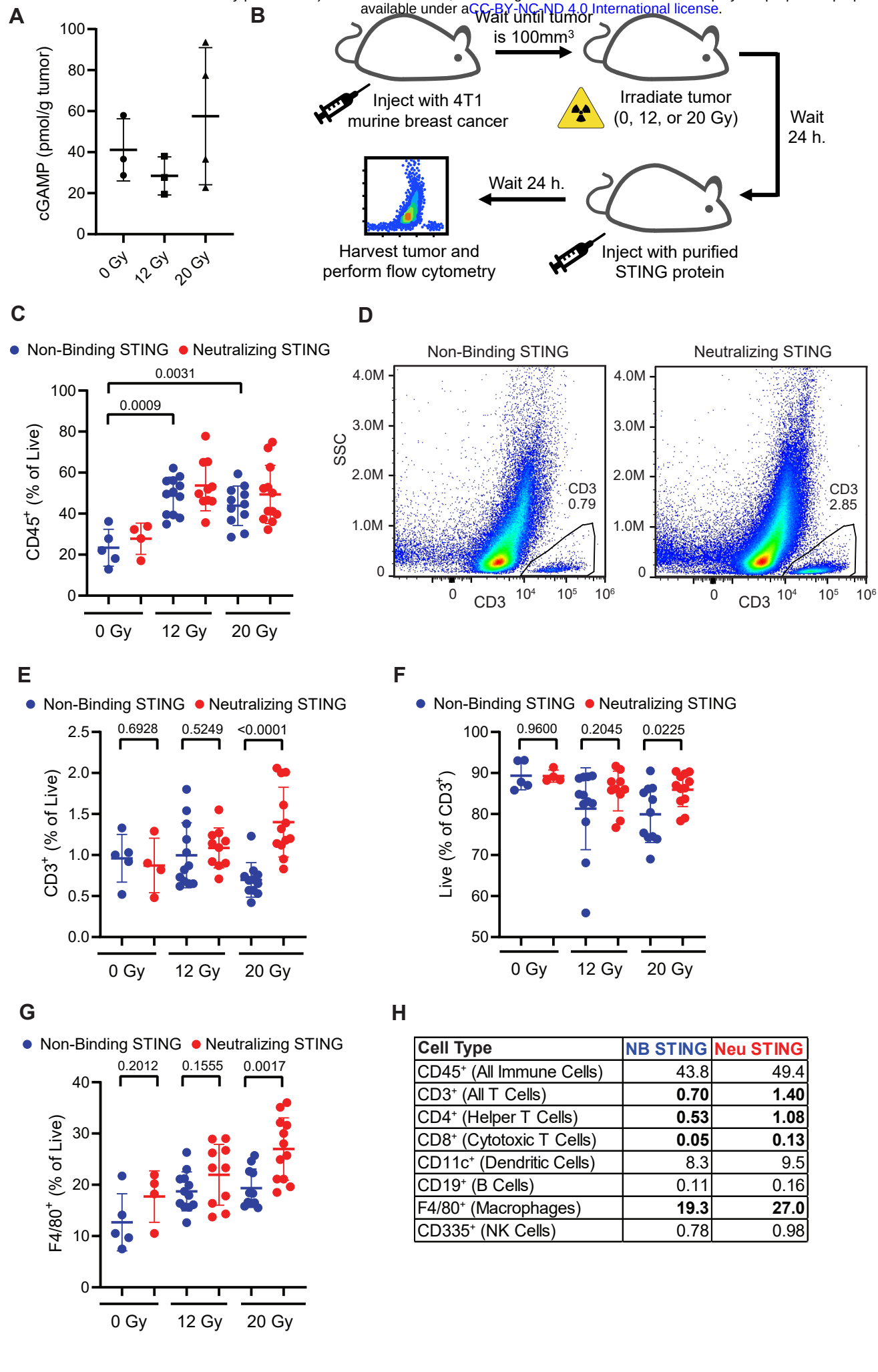

H

Cell Type	NB STING	Neu STING
CD45+ (All Immune Cells)	43.8	49.4
CD3+ (All T Cells)	**0.70**	**1.40**
CD4+ (Helper T Cells)	**0.53**	**1.08**
CD8+ (Cytotoxic T Cells)	**0.05**	**0.13**
CD11c+ (Dendritic Cells)	8.3	9.5
CD19+ (B Cells)	0.11	0.16
F4/80+ (Macrophages)	**19.3**	**27.0**
CD335+ (NK Cells)	0.78	0.98

Figure 2

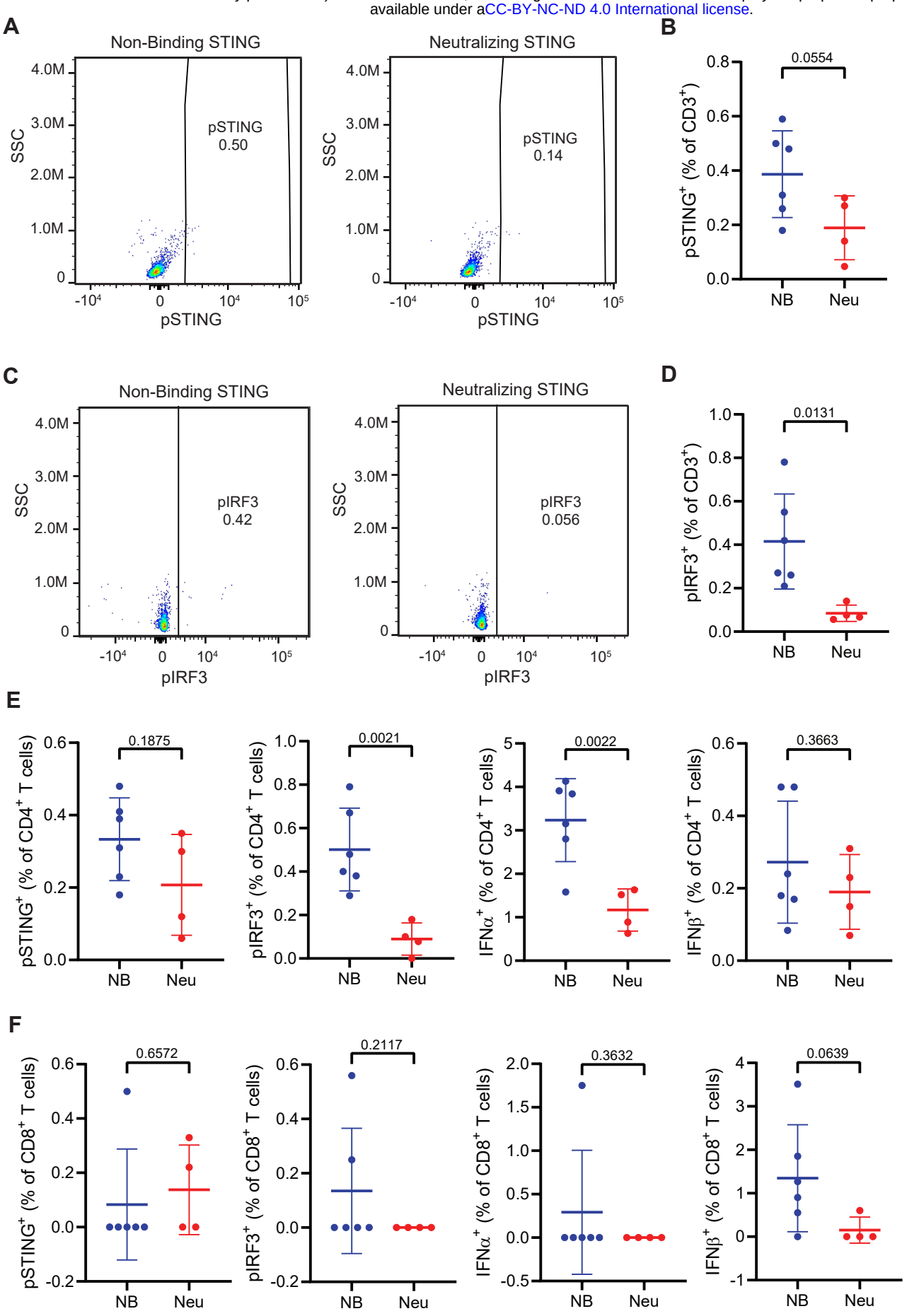

Figure 3

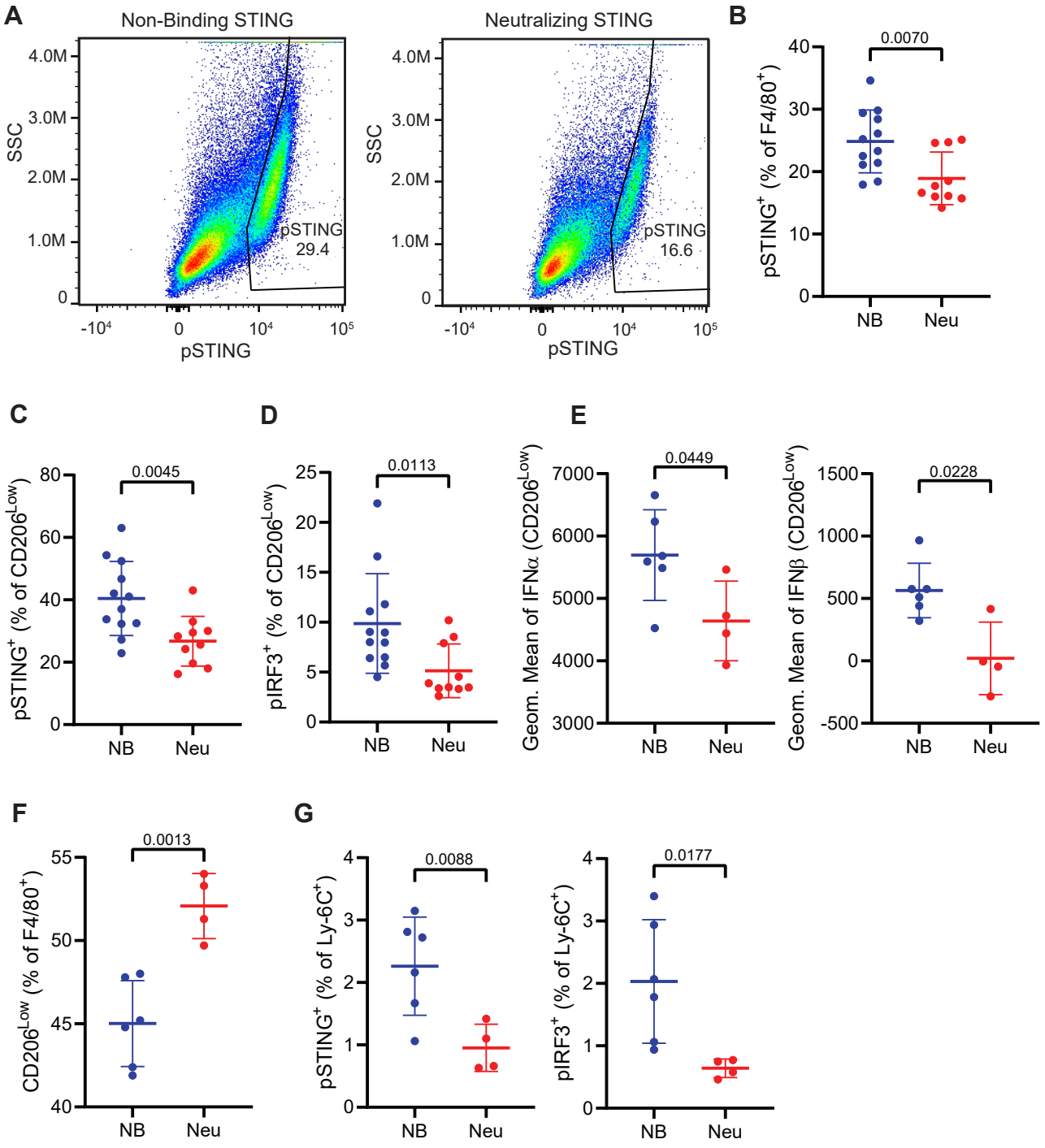

Figure 4

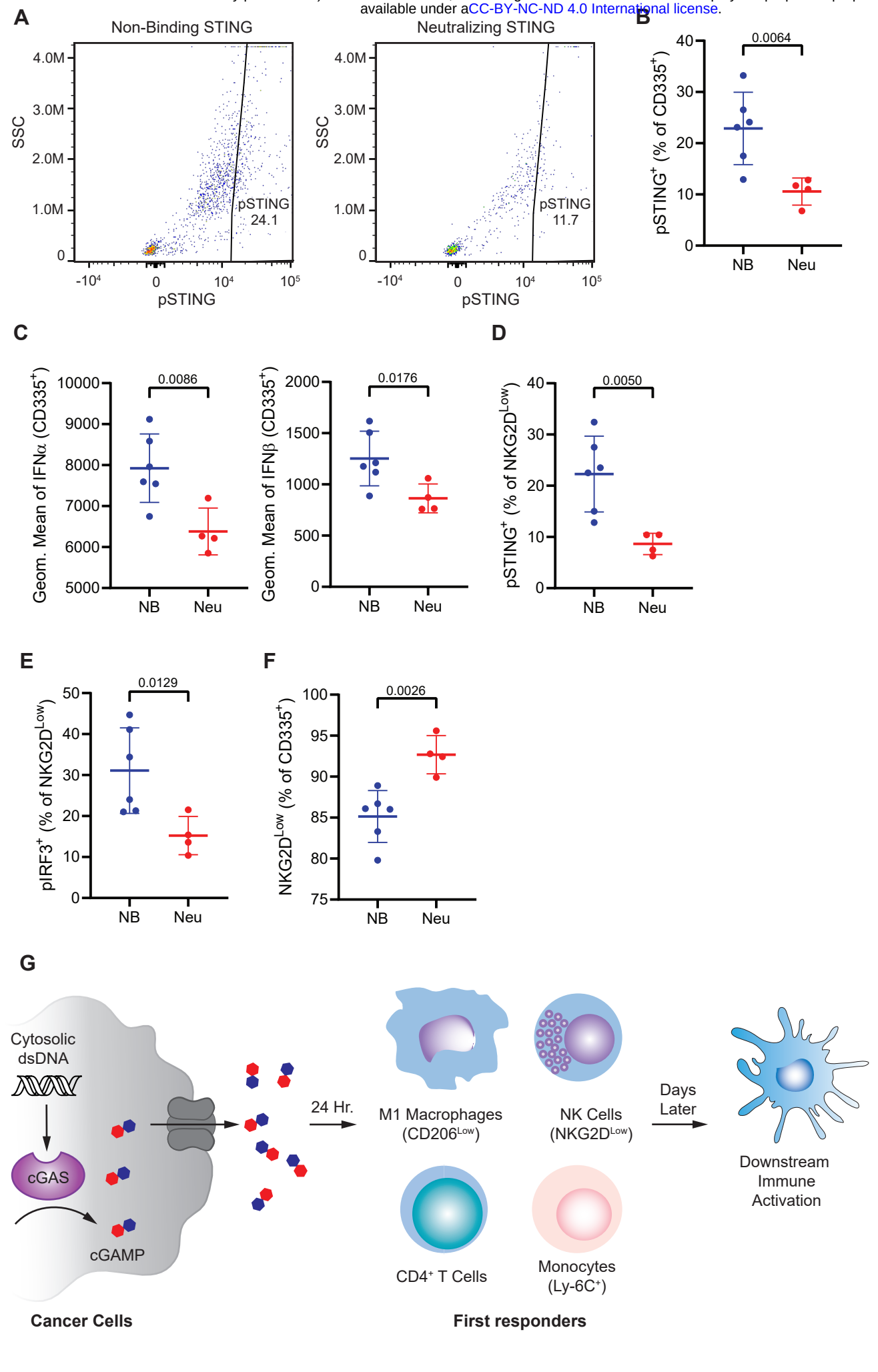

Figure 5

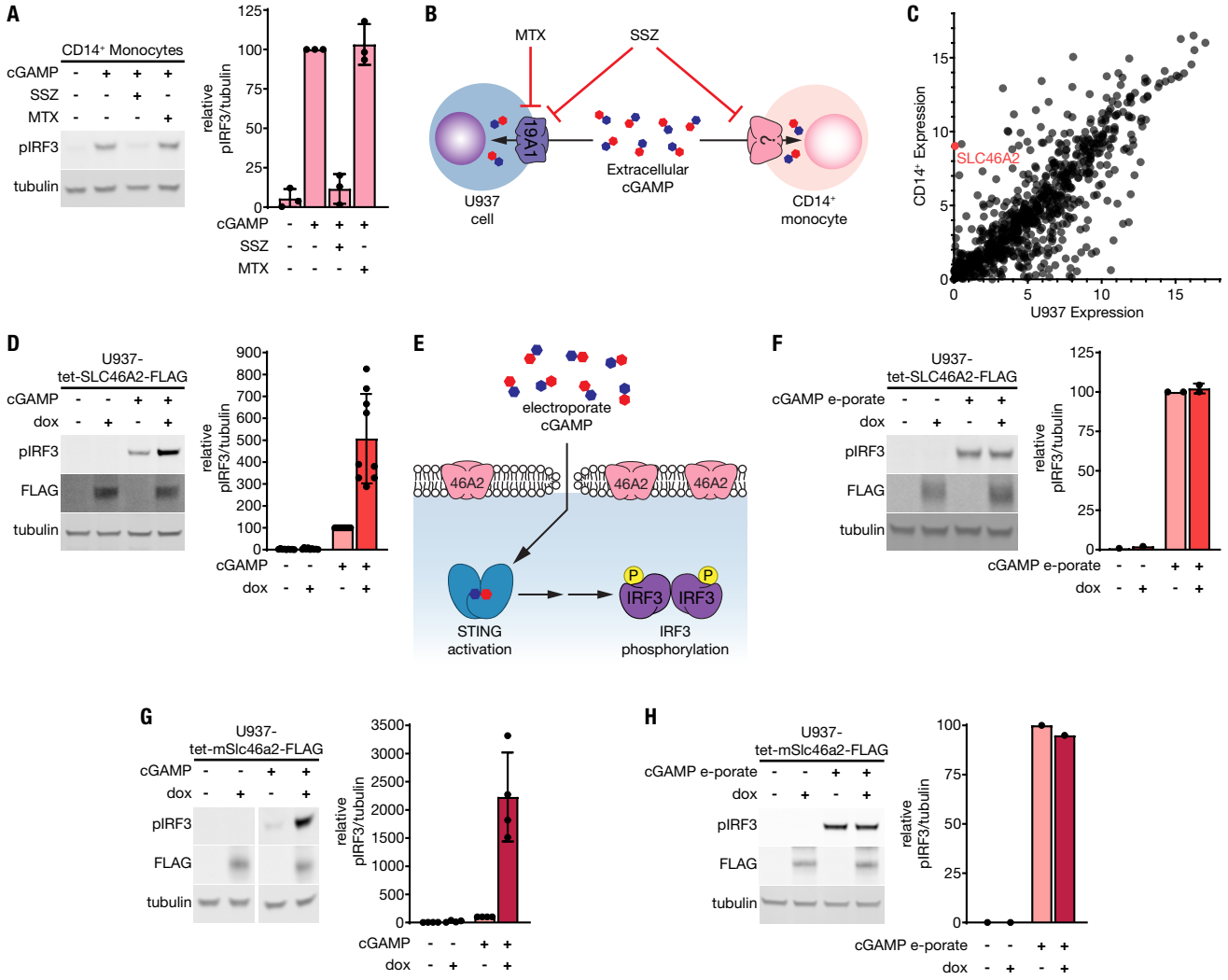
A
CD14⁺ Monocytes
cGAMP
SSZ
MTX
pIRF3
tubulin
relative pIRF3/tubulin
B
MTX
SSZ
19A1
?
Extracellular cGAMP
U937 cell
CD14⁺ monocyte
C
SLC46A2
CD14⁺ Expression
U937 Expression
D
U937-tet-SLC46A2-FLAG
cGAMP
dox
pIRF3
FLAG
tubulin
relative pIRF3/tubulin
E
electroporate cGAMP
46A2
STING activation
IRF3 phosphorylation
P
IRF3
F
U937-tet-SLC46A2-FLAG
cGAMP e-porate
dox
pIRF3
FLAG
tubulin
relative pIRF3/tubulin
G
U937-tet-mSlc46a2-FLAG
cGAMP
dox
pIRF3
FLAG
tubulin
relative pIRF3/tubulin
H
U937-tet-mSlc46a2-FLAG
cGAMP e-porate
dox
pIRF3
FLAG
tubulin
relative pIRF3/tubulin

Figure 6

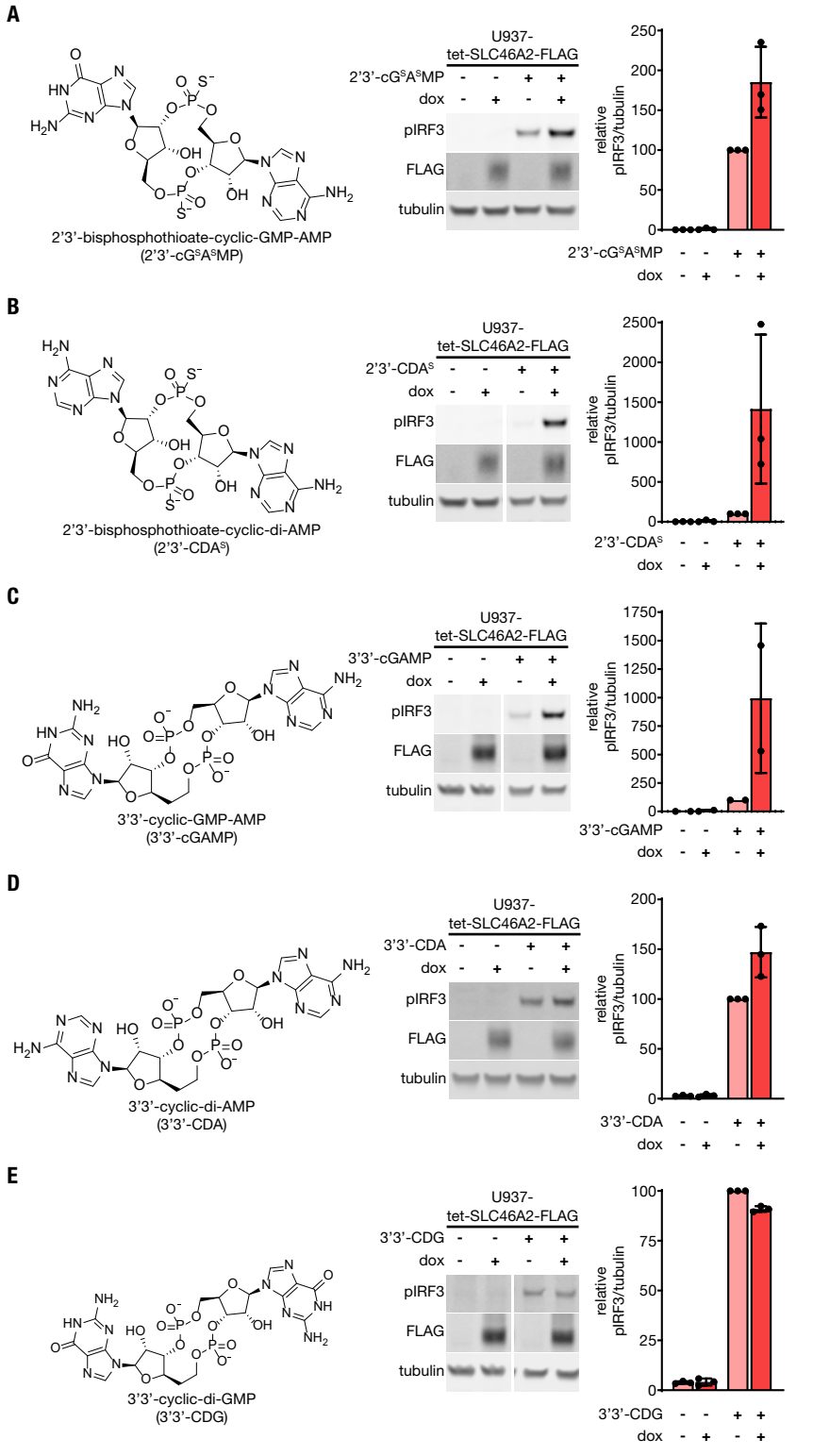
A
2'3'-bisphosphothioate-cyclic-GMP-AMP
(2'3'-cG^{S}A^{S}MP)
U937-
tet-SLC46A2-FLAG
2'3'-cG^{S}A^{S}MP - - + +
dox - + - +
pIRF3
FLAG
tubulin
relative
pIRF3/tubulin
250
200
150
100
50
0
2'3'-cG^{S}A^{S}MP - - + +
dox - + - +
B
2'3'-bisphosphothioate-cyclic-di-AMP
(2'3'-CDA^S)
U937-
tet-SLC46A2-FLAG
2'3'-CDA^S - - + +
dox - + - +
pIRF3
FLAG
tubulin
relative
pIRF3/tubulin
2500
2000
1500
1000
500
0
2'3'-CDA^S - - + +
dox - + - +
C
3'3'-cyclic-GMP-AMP
(3'3'-cGAMP)
U937-
tet-SLC46A2-FLAG
3'3'-cGAMP - - + +
dox - + - +
pIRF3
FLAG
tubulin
relative
pIRF3/tubulin
1750
1500
1250
1000
750
500
250
0
3'3'-cGAMP - - + +
dox - + - +
D
3'3'-cyclic-di-AMP
(3'3'-CDA)
U937-
tet-SLC46A2-FLAG
3'3'-CDA - - + +
dox - + - +
pIRF3
FLAG
tubulin
relative
pIRF3/tubulin
200
150
100
50
0
3'3'-CDA - - + +
dox - + - +
E
3'3'-cyclic-di-GMP
(3'3'-CDG)
U937-
tet-SLC46A2-FLAG
3'3'-CDG - - + +
dox - + - +
pIRF3
FLAG
tubulin
relative
pIRF3/tubulin
100
75
50
25
0
3'3'-CDG - - + +
dox - + - +

Figure 7

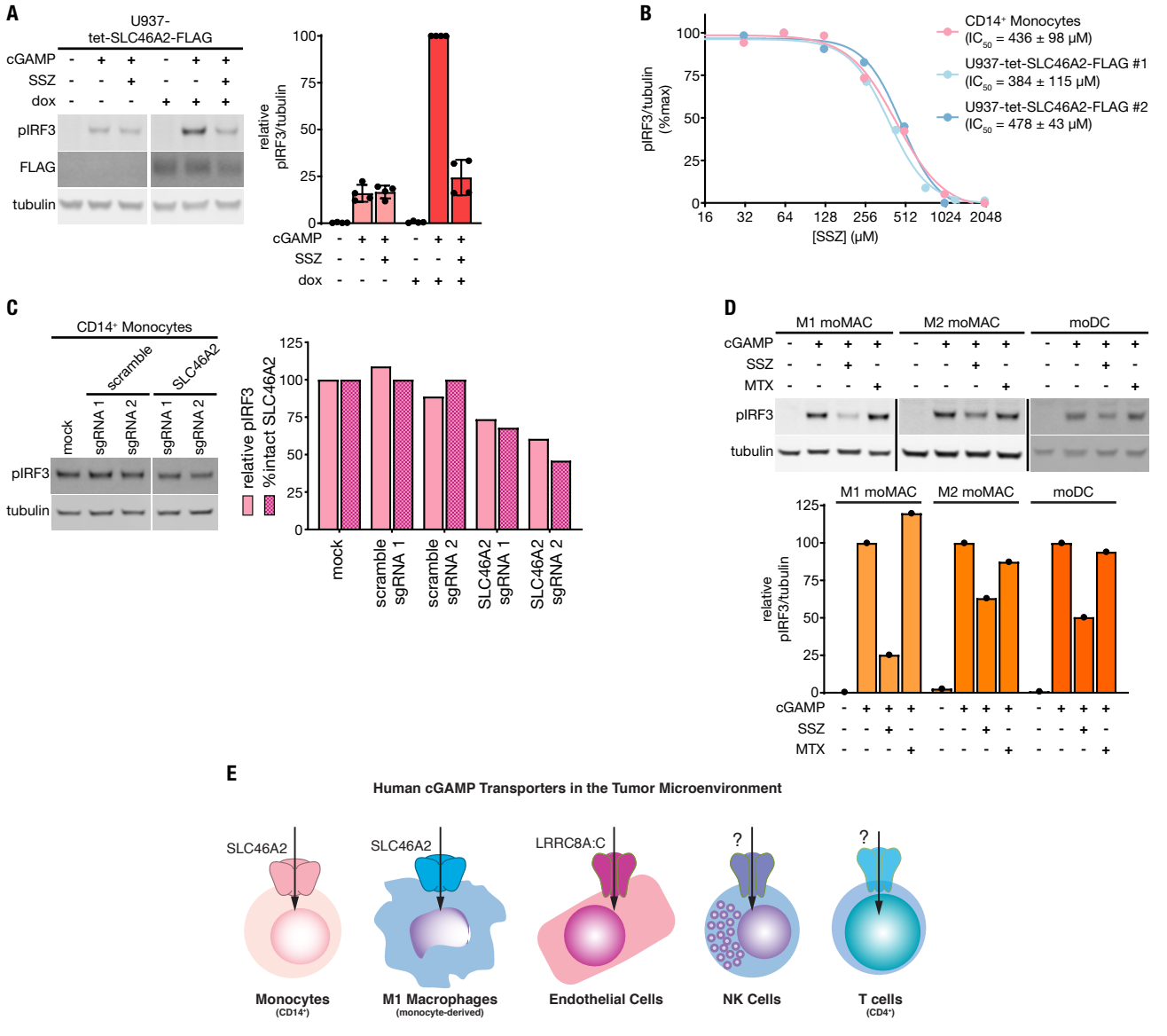
A
U937-tet-SLC46A2-FLAG
cGAMP
SSZ
dox
pIRF3
FLAG
tubulin
relative pIRF3/tubulin
B
CD14+ Monocytes (IC50 = 436 ± 98 μM)
U937-tet-SLC46A2-FLAG #1 (IC50 = 384 ± 115 μM)
U937-tet-SLC46A2-FLAG #2 (IC50 = 478 ± 43 μM)
pIRF3/tubulin (%max)
[SSZ] (μM)
C
CD14+ Monocytes
scramble
SLC46A2
mock
sgRNA 1
sgRNA 2
relative pIRF3
%intact SLC46A2
D
M1 moMAC
M2 moMAC
moDC
MTX
E
Human cGAMP Transporters in the Tumor Microenvironment
SLC46A2
LRRC8A:C
Monocytes (CD14+)
M1 Macrophages (monocyte-derived)
Endothelial Cells
NK Cells
T cells (CD4+)